Sérgio Rhein Schirato

Investigação da utilização da Variabilidade Cardíaca como indicador de estresse fisiológico induzido por exposição a ambientes hiperbáricos e subsequente descompressão

Evaluation of Heart Rate Variability utilization as an indicator of decompression-induced physiological stress

São Paulo

2020

Sérgio Rhein Schirato

Investigação da utilização da Variabilidade Cardíaca como indicador de estresse fisiológico induzido por exposição a ambientes hiperbáricos e subsequente descompressão

Evaluation of Heart Rate Variability utilization as an indicator of decompression-induced physiological stress

Tese apresentada ao Instituto de Biociências da Universidade de São Paulo, para obtenção de Título de Doutor em Ciências, na Área de Fisiologia

Orientador: José Guilherme Chauí-Berlinck

São Paulo

2020

Schirato, S. R.

Investigação da utilização da Variabilidade Cardíaca como indicador de estresse fisiológico induzido por exposição a ambientes hiperbáricos e subsequente descompressão

102 páginas

Tese (Doutorado) – Instituto de Biociências da Universidade de São Paulo, Departamento de Fisiologia

Palavras chave: Variabilidade cardíaca, descompressão, perfis descompressivos,

doença descompressiva, função endotelial, inflamação, sistema imunológico

Comissão Julgadora:

_____

Prof. Dr.

Nome

_____

Prof. Dr.

Nome

_____

Prof. Dr.

Nome

Para Sofia, Eduarda e Leonardo

Agradecimentos

À minha companheira de vida (e de mergulho) Susanne, pelo apoio sempre incondicional, sem o qual este trabalho nunca teria sido possível. Nada que eu escreva aqui fará jus à sua importância na minha vida.

Aos meus pais, que através do seu esforço e exemplo me deram condições para que chegasse até aqui; aos meus irmãos Gabriel e Vitor pelo incentivo, em especial ao Vitor a quem eu tantas vezes pedi opiniões e que indiretamente tornou este trabalho possível.

Aos meus sogros, que tantas vezes deram apoio para que pudesse dedicar o esforço necessário para esta pesquisa.

Um enorme agradecimento ao ZéGui, que (embora tenho certeza de que tenha pensado muitas vezes) em nenhum momento me chamou de lunático ou algo menos educado, pelo contrário, sempre me aconselhou e contribuiu fundamentalmente para que este trabalho fosse realizado. Sem o seu acolhimento, aconselhamento e paciência eu nunca teria chegado até aqui.

Às colegas Vivian e Ingrid, que acordaram de madrugada e passaram incontáveis horas comigo em câmaras hiperbáricas (ainda para piorar, normalmente aos finais de semana) e cuja parceria foi fundamental para a execução deste trabalho. Não tenho palavras para agradecer a contribuição de vocês!

À colega Bruna Bizzarro, que teve paciência para me acolher em seu laboratório e explicar (muitas vezes) como executar uma citometria de fluxo.

A todos os voluntários, alguns amigos de muitos anos, outros que se tornaram amigos neste processo, que muitas vezes enfrentaram horas de viagem com o único propósito de participar desta pesquisa, gentilmente doando seu tempo e sua experiência para que os dados aqui utilizados fossem coletados.

Por fim, agradeço enormemente ao **Centro de Pesquisas Experimentais do Hospital Albert Einstein**, ao **Centro Hiperbárico Paulista** e à **Marinha do Brasil**, que gentilmente cederam suas instalações para que este trabalho fosse realizado.

“Knowing is not enough, we must apply. Willing is not enough, we must do.”

Johann Wolfgang von Goethe

Contents

Appendixes

Resumo

Exposição a ambientes hiperbáricos e subsequente descompressão tem sido associada a diversas alterações fisiológicas, que podem culminar no desenvolvimento de doença descompressiva, uma condição que se manifesta através de diferentes sintomas, variando de dores osteomusculares a distúrbios cardiovasculares e neurológicos, que podem levar à morte. Historicamente estudos sobre descompressão adotaram uma abordagem binária, separando os eventos entre sintomáticos e assintomáticos. Há, porém, um enorme espectro de possíveis alterações fisiológicas entre estes dois extremos, às quais diferentes probabilidades de ocorrência de doença descompressiva podem estar associadas, dependendo de respostas individuais. O objetivo do presente estudo é avaliar a correlação entre marcadores de estresse fisiológico causado pela descompressão, representados por processos inflamatórios, ativação do sistema imunológico e alterações na Variabilidade Cardíaca, verificando se a Variabilidade Cardíaca pode ser usada para estimar o estresse fisiológico causado por um dado perfil descompressivo. Vinte e oito voluntários participaram de dois diferentes protocolos experimentais, divididos em dois perfis diferentes de descompressão, ambos com a mesma pressão máxima e duração, mas com estratégias diferentes de descompressão. Foram realizados, em cada voluntário, eletrocardiogramas e avalições de função endotelial, medida através de Amplitude de Onda de Pulso. Amostras de sangues foram obtidas para: quantificação de hemácias, hemoglobina, hematócrito, neutrófilos, linfócitos, plaquetas, aspartato aminotransferase (AST), alanina aminotransferase (ALT). Imunofenotipagem, quantificação da expressão de mieloperoxidase (MPO) e de micropartículas derivadas de plaquetas, células endoteliais e neutrófilos foram executadas através da utilização de citometria de fluxo. Todos os dados foram obtidos antes e depois de cada protocolo experimental. Os resultados obtidos demonstraram uma clara distinção na quantificação dos marcadores utilizados para identificação de estresse fisiológico relacionado à descompressão nos dois perfis decompressivos utilizados. Há uma associação entre redução na Variabilidade Cardíaca, produção de micropartículas e marcadores de ativação de neutrófilos. O perfil descompressivo com paradas de descompressão efetuadas a pressões ambientes maiores está

associado a maiores contagens de micropartículas e ativação de neutrófilos, quantificada pela expressão de MPO, e com maior redução da Variabilidade Cardíaca e função endotelial.

Palavras chave: Variabilidade cardíaca, ambientes hiperbáricos, descompressão, perfis descompressivos, doença descompressiva, função endotelial, inflamação, sistema imunológico

Abstract

Exposure to hyperbaric environments and subsequent decompression has been associated with many physiological alterations, which may culminate in decompression sickness, a disease that might manifest itself through a variety of symptoms, ranging from joint and/or musculoskeletal pain, to cardiovascular and neurological impairment and, ultimately, death. Historically, decompression studies have adopted a binary approach, separating post decompression events between symptomatic and asymptomatic. There is, however, a huge spectrum of possible physiological alterations between these two extremes to which probabilities of decompression sickness occurrence are likely to be associated, based on individual responses. The purpose of this study is to analyze the correlation between decompression-related physiological stress markers, given by inflammatory processes and immune system activation and changes in Heart Rate Variability, evaluating whether Heart Rate Variability can be used to estimate the physiological stress caused by a given decompression profile. A total of 28 volunteers participated in two different experimental protocols, divided in two different compression-decompression profiles, both with same maximum pressure and duration, but with different decompression schedules. Electrocardiograms and endothelial function evaluations, measured through Pulse Wave Amplitude were performed; blood samples were obtained for the quantification of red cells, hemoglobin, hematocrit, neutrophils, lymphocytes, platelets, aspartate transaminase (AST), alanine aminotransferase (ALT), and for immunophenotyping and microparticles (MP) research through Flow Cytometry, before and after each experimental protocol from each volunteer. Also, myeloperoxidase (MPO) expression and microparticles (MPs) deriving from platelets, neutrophils and endothelial cells were quantified. The results obtained demonstrated a clear distinction between the outcomes of the different decompression profiles in most indicators used to quantify decompression-related physiological stress. There is an association between HRV reduction and MPO, MPs production, platelet count and neutrophils activation markers. The decompression profile with decompression stops at higher ambient pressures was associated with higher counts of MPs and neutrophil

activation, quantified by MPO expression in addition to reduced HRV and endothelial function.

Keywords: Heart Rate Variability, hyperbaric environments, decompression, decompression profiles, decompression sickness, endothelial function, inflammation, immune system

Introduction

Since the first animal experiments involving decompression made in the 17th century by Robert Boyle, the desire to understand and control the adverse physiological consequences derived from changes in the environment hydrostatic pressure (initially mainly due to underwater incursions, later in civil construction and more recently in the aerospace exploration) has attracted the attention of researchers.

In the 19th century, the development of diving bells, the military dependent diving technologies and the utilization of underwater rooms in civil construction have dramatically increased the occurrence of what became known as decompression sickness ("DCS"). DCS is a disease associated with the exposure to hyperbaric environments, or more precisely, with the subsequent decompression, that could manifest itself through a variety of symptoms, ranging from joint and/or musculoskeletal pain, to cardiovascular and neurological impairment and, ultimately, death. This development created demand for a systematic approach in the search for a way to manage the problem.

The first comprehensive attempt to understand the illness related to the exposure to hyperbaric environments was led by John Scott Haldane in collaboration with Arthur Edwin Boycott and Guybon Chesney Castell Damant, and published early in the 20th century [1].

In retrospect, the methodology used in their study, the assumptions that different tissues would absorb and eliminate gas at different rates and how they modeled it, and the arguments used against the linear decompression (a method widely used at the time) are remarkable, especially if the knowledge and resources available at the time are taken into consideration. In many respects, most of Haldane's conclusions remain the basis for many procedures still in use today. With a few improvements to supersaturation values, and other refinements (or "fit-to-reality adjustments"), the differential equations used by Haldane are the same ones used in almost every computer or software available on the market today for decompression calculation.

Given the information that was available at the time, it is understandable that Haldane and his coworkers treated the matter as a physical (or mechanical) problem caused by bubbles forming during decompression. Having said that, it is worthwhile to note that in their study, they specifically recognized that many of the animals that died did not reveal signs of bubbles during necropsy and Haldane speculated that bubbles might have formed in parts of the body they did not study.

Nevertheless, he laid the foundation for an idea that is still very much accepted: decompression sickness is a mechanical problem caused by bubbles formed during decompression.

For many years it was believed that bubbles were related to decompression sickness and that their absence would mean a successful decompression. However, with the development of Doppler ultrasound technology late in the 1970s, it became clear that even mild exposures to hyperbaric environments and subsequent decompression would lead to bubble formation in the venous circulation. Though bubbles were commonly found in the right chambers of the heart, Doppler echocardiograms showed that most of them were filtered by the lungs and were not observed in the left chambers of the heart. In theory, bubbles would be pumped from the left chambers into the systemic circulation, which would send them to the central nervous system, causing the neurological symptoms of decompression sickness. This finding led to the endless discussion about the role of cardiac or pulmonary shunts in decompression sickness since the existence of a shunt would allow the migration of bubbles from the venous to the arterial (i.e., systemic) circulation, bypassing the filtering effect of the lungs.

While this statement might hold true for large venous gas emboli most of the time [2 3], there are other facts that must be considered: (i) Patent Foramen Ovale (PFO), a remain from our fetal circulation, is found in approximately one-third of the population [4]; (ii) pulmonary

shunts are, among other things, a physiological response to handle the cardiac afterload, and studies with high-performance athletes have shown that all subjects studied presented some level of pulmonary shunting as the physical effort to which they were submitted increased [5]; (iii) the central nervous system has fast inert gas kinetics [6], meaning that bubbles eventually shunted through the heart to these tissues tend to lose gas to the media, being reduced in size and quickly collapsing. This assumption can be supported by the fact that the gold standard for PFO detection is the transesophageal echocardiogram coupled with the injection of agitated saline solution, in which gas serves as a contrasting media to the ultrasound. There are no known cases of decompression sickness-like symptoms related to the use of such contrast, even when bubbles are clearly shunted to the left atrium.

Additionally, post-dive bubbles detected by standard echocardiograph have diameters larger than 30 μm. A recent study using contrast-enhanced imaging techniques capable of detecting bubbles with diameters smaller than 10 μm indicated the presence of smaller emboli in both sides of the heart [7], demonstrating that: (i) there are small bubbles in humans that are not filtered by the lungs; (ii) there are small bubbles even in the absence of larger venous gas emboli; and (iii) smaller bubbles follow a different timeline than larger venous gas emboli. Bubbles forming in the arterial circulation have also been identified in previous studies though their role in decompression sickness, especially in the presence of neurological symptoms, is yet to be understood. Vascular bubble models, designed to study nucleation on a flat hydrophobic surface and how they expand to form bubbles after decompression, hold great promise for the improvement of decompression procedures in the future [8].

As it will be discussed in this study, several reports over the past two decades have shown that exposure to hyperbaric environments and subsequent decompression has many physiological implications, ranging from reduction in endothelial function to activation of the immune system [9] [10] [11]. As mentioned above, post decompression formation of bubbles is a common finding in subjects exposed to hyperbaric environments. Due to large inter-personal variability [12], venous gas emboli are, however, a poor surrogate for decompression sickness [13], and the causal relationship between them and other decompression-related

physiological alterations, if any, is yet to be understood [14]. In recent years, the endothelial dysfunction hypothesis [15], which postulates that microparticles associated with endothelial damage may act as nucleation sites for bubble formation, has drawn attention and gained support. This hypothesis is based on the recently accumulated knowledge about small particles (microparticles or microvesicles) shed by different cells in an organized and regulated manner. Such microparticles (MPs), which carry various nuclear components of their originating cells, like RNA and DNA, are involved in cell signaling and communication, and have recently emerged as relevant markers of inflammatory diseases [16]. Variations in their levels and the cells from where they were originated have been linked to an increasing range of diseases and inflammatory processes [17] [18]. This has resulted in decompression sickness being seen not as merely a physical or mechanical problem, but instead as a result of a complex biochemical process.

In this sense, one recently published study has shown that the exposure to high-pressure environments, even in the absence of decompression, is sufficient to increase the production of MPs carrying IL-1β [19] an interleukin that belongs to cytokines, which is an important mediator in inflammatory responses. The same study demonstrated that individuals exposed to higher ambient pressures produced a higher average count of MPs after the dive, which persisted for at least 2 hours after the end of the dive, while the changes observed in the group exposed to lower ambient pressure resolved within 2 hours after the dive.

The mechanism behind the formation of such microparticles has been described as related to high inert gas pressure through a mechanism that causes singlet oxygen formation, a potentially toxic free radical initiated by a cycle of actin S-nitrosylation, nitric oxide synthase-2, and NADPH oxidase activation ultimately leading to microparticle formation [20]. The potential to trigger this reaction depends on the gas and follows the rank: argon ~ nitrogen > helium. This ranking might explain the reduced endothelial dysfunction, as defined below, identified after hyperbaric exposures where helium was part of the breathing mix [21] and the increased MP production related to exposure to elevated partial pressures of nitrogen in comparison to elevated partial pressures of oxygen [22].

The endothelium, a monolayer of endothelial cells, constitutes the inner cellular lining of the blood vessels (arteries, veins and capillaries) and the lymphatic system, and therefore is in direct contact with the blood/lymph and the circulating cells [23]. Endothelial function might be described as: (i) the capacity of the vascular endothelium to respond to vasodilator stimulus, in a series of mechanisms mediated both by nitric oxide (NO) and non-NO pathways; (ii) controlling for leukocyte adhesion, smooth muscle cell growth and platelet aggregation [24] . Endothelial dysfunction is associated with many cardiovascular diseases [25].

Despite their harmful effects to the host, the production of reactive oxygen species (ROS) is part of an orchestrated physiological response of the immune system to stop bacteria and fungus. As described above, exposure to high inert gas pressures, even in the absence of decompression, is apparently linked to an increased production of ROS. The NADPH oxidase, due to neutrophils activation, causes the generation of ROS that are originated by their heme enzyme (defined as enzymes that catalyze the oxidative chemical transformation of a substrate) myeloperoxidase (MPO) [26]. Therefore, it is expected that higher expressions of MPO are linked to the generation of ROS and ultimately, due to the mechanism described above, microparticles. In fact, it has been demonstrated that individuals suffering from decompression sickness present higher levels of circulating MPs, as well as levels of MPO expression, for long periods after the appearance of the symptoms, although altered levels of such markers are also observed in symptom free individuals that were submitted to hyperbaric exposure. It seems, however, that in symptom free individuals the time for the resolution of the alterations is shorter and the changes magnitude is lower [10].

The vascular endothelium, while regulating the passage of macromolecules and circulating cells from blood to tissues, is a major target of oxidative stress. ROS are known to reduce the availability of NO, the most important endothelial-derived factor, due to, among other mechanisms, their role in the production of asymmetric dimethyl-L-arginine (ADMA), an endogenous inhibitor of NO synthase [27]. This reduction in the endogenous levels of NO is probably the cause of the well documented loss of endothelial function in individuals submitted to a compression-decompression process [28 29].

Based on the assumption that decompression sickness is associated with the oxidative stress described above, over time, different studies evaluated whether the ingestion of diverse anti-oxidant aliments or supplements, varying from dark chocolate to vitamin C, would reduce the dive related endothelial dysfunction and MP production [30] [31]. Although there are apparently benefits, whether it would translate in a lower incidence of decompression sickness remains unclear.

Interestingly, different studies with murine models and humans have demonstrated that increased endogenous levels of NO provoked by aerobic exercise prior to hyperbaric exposure reduced the incidence of decompression sickness and the mortality due to decompression sickness after provocative decompression in rats [32], and the production of MPs and endothelial dysfunction in humans [33]. In the same manner, when NO synthase is inhibited using L-Name (a non-selective NOS inhibitor), the survival rate was greatly reduced among rats exposed to hyperbaric pressure and subsequent decompression, reinforcing the understanding that NO and oxidative stress play an important role in the decompression sickness.

With divers pushing the boundaries of deeper diving beyond military and commercial diving, and the introduction of helium in the breathing mixes in the 1990s, different decompression techniques for bounce (non-saturation) dives started to be tested. Richard Pyle, an American ichthyologist from Hawaii, was probably one of the first to publicly advocate for decompression stops deeper than those calculated by algorithms derived from Haldane´s theory. On dives ranging in depth from 40 to 70 m, he correlated catching fishes with his overall feeling after diving, and attributed feeling better to the fact that when a fish was caught, he had to stop much deeper than determined by decompression algorithms to release gas out the fish´s swim bladder. Decompression algorithms based on the control of bubble formation and growth including the Varying Permeability Model developed by David Yount, which is the most well-known algorithm based on this strategy (probably because it is open code software), require decompression stops at greater depths, corroborating Richard Pyle´s conclusions. At some point, it became well-established within the diving community that deeper stops were mandatory and even Albert Bühlmann´s ZHL

16 algorithm was adjusted; gradient factors (a way to arbitrarily adjust the linear function used to determine gas supersaturation limits in theorical compartments) were implemented to force the algorithm to produce deeper stops.

There is, however, no scientific data available to support the belief that the modification of the decompression schedule with the inclusion of deeper stops reduces the expected probability of decompression sickness. In reality, studies showed that slower ascents are related to higher counts of bubbles upon surfacing [34]. Nevertheless, whether this translates to a higher probability of decompression sickness is another matter.

In what was probably the largest study comparing the incidence of decompression sickness in bubble-based models versus dissolved gas-based models (derived from Haldane's work), the US Navy Experimental Diving Unit [35] concluded that decompression schedules with deeper stops had higher incidence of decompression sickness. In this study, dive profiles with equal decompression times and to a depth of 51 m were calculated using each model. These were then compared for decompression sickness and venous gas emboli count. The deep stops schedule resulted in a significantly higher incidence of decompression sickness than the shallow stops schedule (10 cases versus 3, a result significant at the 5% level of confidence). Interestingly, the bubble-based profile resulted in a higher maximum venous gas emboli grade count, as well as higher average grade count.

The reason behind the findings mentioned above might be related to the different supersaturation observed in the tissues with slower gas kinetics upon surfacing. Figure 1 illustrates total inert gas in each tissue upon surfacing, based on Albert Bühlmann´s ZHL 16 algorithm, for two profiles calculated with different gradient factors (GF) to simulate decompression schedules generated by dissolved gas- and bubble-based models.

Both profiles were calculated in order to provide similar decompression times for a dive to 51 meters of depth and a bottom time of 30 minutes. As it can be seen, the profile with deeper stops generated higher supersaturation values in the slower compartments upon

surfacing, while the profile without deeper stops generated higher supersaturation values in the faster compartments, which, assumedly, tolerate higher inert gas pressures.

Probably, a better way to compare these two decompression schedules would be to compare the supersaturation in a given compartment produced by each one, by subtracting the ambient pressure from the total inert gas pressure in a compartment (all calculations were made using an ambient pressure of 1 atmosphere). In Figure 1 it can be identified that only compartments 6 to 15 have internal inert gas pressures higher than ambient pressure upon surfacing (meaning that compartments 1 to 5 and 16 had total inert gas pressures below ambient pressure upon surfacing).

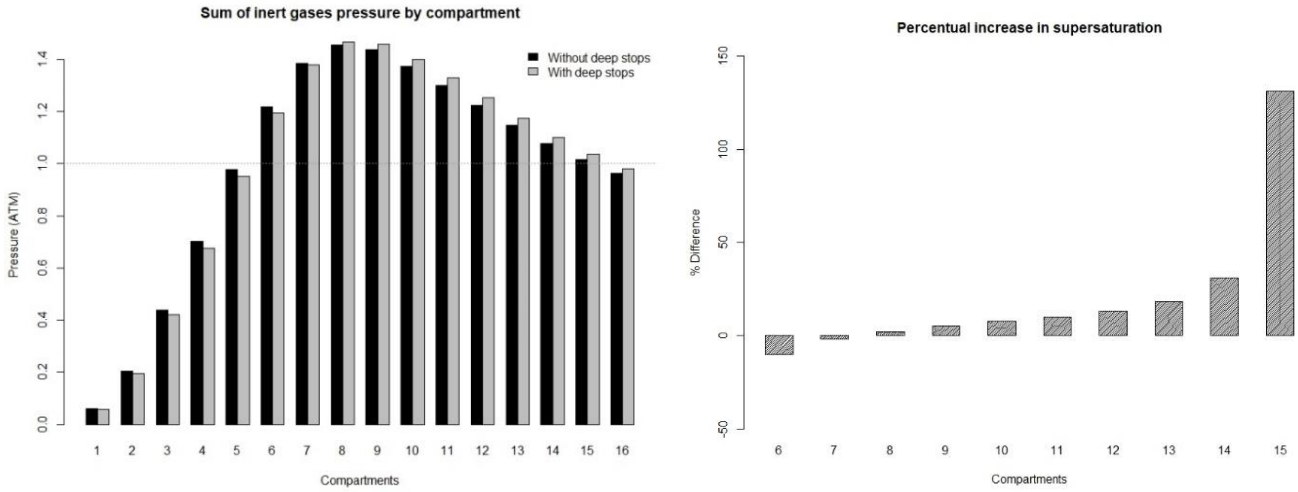

Figure 1. Total inert gas pressure in each compartment at the end of the dive and percent increase in supersaturation between profiles

It is easy to notice that the decompression schedules with deeper stops generated supersaturation values as high as 2.3 times the supersaturation produced by the profile with shallower stops. This difference might be a possible explanation for the conclusions from the studies previously mentioned that associated deeper decompression stops with higher incidence of decompression sickness.

Besides the well documented appearance of bubbles, alterations in the endothelial function, with related biochemical markers found in the blood stream, and the development of immune system activation that, ultimately might play an important role in decompression sickness, which all have been extensively described, as previously mentioned, recently published studies also reported changes in the Heart Rate Variability (HRV) after exposure to hyperbaric environments [36] [37]. The present study hypothesize that such changes might be related to decompression-induced physiological stress and, ultimately, with the endothelial and immune function alterations previously reported.

Heart Rate Variability is defined as the undirected changes in the interval between successive normal (triggered by the sinus node) heartbeats. Usually, this is assessed through the timing between QRS complexes in a continuous electrocardiograph recording (ECG). It is the result of the balance between the sympathetic and the parasympathetic branches of the autonomic nervous system (ANS) [38], as well as of other non-neural sources of variation. The parasympathetic influence on the heart is mediated via release of acetylcholine. Muscarinic acetylcholine receptors respond to this release by increasing the cell membrane conductance to K^+. Conversely, the sympathetic influence is mediated by the release of epinephrine and norepinephrine. Activation of β-adrenergic receptors result in cyclic AMP mediated phosphorylation of membrane proteins, causing an acceleration of the slow diastolic depolarization. The vagal and sympathetic activity constantly interact. As the sinus node is rich in acetylcholinesterase, the effect of a vagal impulse is brief because the acetylcholine is rapidly hydrolyzed. Parasympathetic influences exceed sympathetic effects probably via two different mechanisms: a cholinergically induced reduction of norepinephrine released as response to sympathetic activity, and a cholinergic attenuation of the response to an adrenergic stimulus.

HRV is commonly studied in the time and frequency domains, and eventually through the application of non-linear methods, which will not be discussed in this study [38]. Different HRV indicators have been associated with sympathetic or parasympathetic activity. For instance, for many years it has been believed that the Lower Frequencies of the spectrogram, a frequency domain indicator, were related to the sympathetic activity, while the Higher

Frequencies were related to the parasympathetic branch of the ANS. In reality, the association between a given wave width and one specific branch of the ANS is probably not so well defined, and there are probably other factors contributing in the process. Higher Frequencies are highly impacted by respiratory pattern, while Lower Frequencies are affected by both, the sympathetic and the parasympathetic branches of the ANS [39]. Additionally, an association between the Lower Frequencies and the baroreflex function has been made by at least one study [40]. The quantification of the sympathetic and parasympathetic nervous activities has been made through the utilization of the Principal Dynamic Mode method (PDM), with apparently more precise estimation of the activity of each branch of the ANS [41], but, due to the nature of the method, the participation of other contributing factors is ignored. This study will not apply nor discuss the application of the PDM method to differentiate between the activities of the two branches of the ANS.

A reduction in HRV has been reported in several cardiological and non-cardiological diseases, ranging from diabetes to renal failure, to mention a few [42] [43] [39]. A reduction in HRV, when analyzed in the frequency domain has also been associated with inflammatory processes by more than one study [44] [45].

Since there is an undisputable contribution of inflammatory processes and immune responses to the final result of the compression and subsequent decompression processes, based on the associations described above, HRV study in this specific context might bring important contributions to the understanding of the underlying physiological processes and potential outcomes of exposures to hyperbaric environments.

Objective of this research

The purpose of this study is to further explore previous results obtained in the Laboratory of Energetics and Theoretical Physiology of the University of Sao Paulo, by increasing the number of physiological indicators observed and their association with the success of the compression – decompression process.

Historically, decompression studies have adopted a binary approach, separating events between symptomatic and asymptomatic. There is, however, a huge spectrum of possible alterations between these two extremes to which probabilities of decompression sickness occurrence are likely to be associated, based on individual responses.

The ultimate objective of this study is to quantify and model these individually observed alterations, aiming to answer two questions: (i) can HRV be used to estimate the physiological stress caused by a given decompression profile; and (ii) based on the first answer, would it be possible to adjust a decompression profile on an individual basis, in order to reduce the likelihood of decompression sickness based on individual susceptibility.

It is known that different individuals respond differently to the compression – decompression process, with some being more prone to develop symptoms of decompression sickness. By keeping track of different physiological stress markers, this study is designed to lay the ground for a different approach to the problem. Instead of trying to determine supersaturation limits associated to a given probability of appearance of decompression sickness symptoms for a given exposure profile, the follow on research will focus on the creation of a model used to predict individual responses to certain exposures, allowing for the adjustment of the profile in accordance to the modeled impacts. In this sense, the study of individual responses, in special HRV pre and post exposure variations, herein described will be an extremely valuable asset.

Materials and Methods

The present study was undertaken in healthy individuals, all trained divers, experienced in the experimental profiles utilized. All provided a written informed consent. The ethical committee of the Biosciences Institute of the University of Sao Paulo approved the experimental protocol (CAAE #91231618.6.0000.5464).

Simulated dives

Approximately 180 hours-man of experiments involving exposure to hyperbaric environment and subsequent decompression were conducted at three different facilities: (i) the hyperbaric chamber at the Centro Hiperbárico Paulista, (ii) the Brazilian Navy hyperbaric chamber at the Centro de Instrução e Adestramento Almirante Átilla Monteiro Aché (CIAMA) facility, and (iii) the Y-40 swimming pool located in Therme de Montegrotto, Italy, under the coordination of DAN Europe. All experiments were executed under the supervision of a trained physician.

Each volunteer underwent two different trials, each one with the same maximum depth and bottom time. Decompression schedules were created to simulate different decompression profiles, keeping, however, similar total decompression times. Total inter gas supersaturation was computed and defined to be approximately equal in equivalent decompression profiles, even for simulated dives executed at different facilities.

Each trial was performed in the morning, at the same time of the day, and the interval between the experiments was at least seven days for each volunteer, in order to minimize any carry-over effect. The only exception were the two experiments at the Y – 40 Swimming Pool that happened only two days apart from each other and in different times of the day, due to logistical challenges.

The experiments executed at the Centro Hiperbárico Paulista were performed using electronically controlled closed-circuit rebreathers, while the experiments performed at the navy facility used breathing gas supplied through the chamber's built-in breathing system (BIBS) and the volunteers that participated in the Y- 40 experiment used self-contained breathing apparatus (SCUBA).

The Simulated Dive Profiles

Centro Hiperbárico Paulista

All volunteers used electronically controlled closed-circuit rebreathers. The gas chosen as diluent consisted in a mix of 18% oxygen, 45% helium and 37% nitrogen and the rebreathers were set to keep the oxygen pressure at 121 kPa (1.2 ATA – total pressure: gauge plus 0.93 atm of surface pressure) throughout the dive, raising the oxygen pressure to 141 kPa (1.4 ATA) at 162 kPa (6 msw – meters of sea water). The experimental pressure was 638 kPa (53 msw). The time required to reach the experimental pressure was 20 minutes and the divers were kept at this pressure for 15 additional minutes. Subjects were decompressed at a rate of 9 msw/min until the first decompression stop was reached. Dive profiles are detailed below (Table 1).

Table 1. *Centro Hiperbárico Paulista Dive Profiles*

Deeper Stops Profile			Shallower Stops Profile		
Depth (msw)	Time (minutes)	Breathing Loop PO2 (ATA)	Depth (msw)	Time (minutes)	Breathing Loop PO2 (ATA)
53	15	1.2	53	15	1.2
27	1	1.2	21	2	1.2
24	1	1.2	18	2	1.2
21	2	1.2	15	3	1.2
18	2	1.2	12	4	1.2
15	3	1.2	9	6	1.2
12	4	1.2	6	26	1.4
9	5	1.2			
6	23	1.4			

Navy Facility - Centro de Instrução e Adestramento Almirante Átilla Monteiro Aché (CIAMA)

Breathing gas was supplied through the chamber's built-in breathing system (BIBS). The time required to reach the experimental pressure was 15 minutes. The breathing gases consisted in a mix of 15% oxygen, 55% helium and 30% nitrogen at a pressure of 861 kPa (75msw) for a 10 minutes bottom time. Subjects were decompressed at a rate of 9 msw/min until the first decompression stop. At a pressure of 324 kPa (21 msw) the breathing gas was changed to 50% oxygen and 50% nitrogen. At 162 kPa (6 msw) the breathing gas was changed to pure oxygen, which was used until the end of the dive. Dive profiles are detailed below (Table 2).

Table 2. *CIAMA Dive Profiles*

Deeper Stops Profile			Shallower Stops Profile		
Depth (msw)	Time (minutes)	Breathing Gas Composition	Depth (msw)	Time (minutes)	Breathing Gas Composition
75	10	15% O_2 / 55% He / 30% N_2	75	10	15% O_2 / 55% He / 30% N_2
42	2	15% O_2 / 55% He / 30% N_2	33	2	15% O_2 / 55% He / 30% N_2
39	1	15% O_2 / 55% He / 30% N_2	30	2	15% O_2 / 55% He / 30% N_2
36	2	15% O_2 / 55% He / 30% N_2	27	3	15% O_2 / 55% He / 30% N_2
33	2	15% O_2 / 55% He / 30% N_2	24	3	15% O_2 / 55% He / 30% N_2
30	2	15% O_2 / 55% He / 30% N_2	21	3	50% O_2 / 50% N_2
27	3	15% O_2 / 55% He / 30% N_2	18	3	50% O_2 / 50% N_2
24	4	15% O_2 / 55% He / 30% N_2	15	4	50% O_2 / 50% N_2
21	3	50% O_2 / 50% N_2	12	6	50% O_2 / 50% N_2
18	3	50% O_2 / 50% N_2	9	10	50% O_2 / 50% N_2
15	4	50% O_2 / 50% N_2	6	35	100% O_2
12	5	50% O_2 / 50% N_2			
9	9	50% O_2 / 50% N_2			
6	30	100% O_2			

Y – 40 Swimming Pool

All volunteers used SCUBA. The breathing gases consisted in a mix of 21% oxygen, 35% helium and 44% nitrogen at a pressure of 528 kPa (42msw) for a 40 minutes bottom time. The divers descended at a rate of approximately 20 msw/min, reaching the bottom of the water column in approximately 2 minutes. Subjects were decompressed at a rate of 9

msw/min until the first decompression stop. At a pressure of 324 kPa (21 msw) the breathing gas was changed to a mix of 50% oxygen and 50% nitrogen. Dive profiles are detailed below (Tables 5 and 6).

Table 3. *Y - 40 Swimming Pool Dive Profiles*

Deeper Stops Profile			Shallower Stops Profile		
Depth (msw)	Time (minutes)	Breathing Gas Composition	Depth (msw)	Time (minutes)	Breathing Gas Composition
42	40	21% O_2 / 35% He / 44% N_2	42	40	21% O_2 / 35% He / 44% N_2
21	4	50% O_2 / 50% N_2	9	4	50% O_2 / 50% N_2
18	3	50% O_2 / 50% N_2	6	27	50% O_2 / 50% N_2
15	3	50% O_2 / 50% N_2			
12	3	50% O_2 / 50% N_2			
9	9	50% O_2 / 50% N_2			
6	14	50% O_2 / 50% N_2			
3	5	50% O_2 / 50% N_2			

Although recorded and processed, the data obtained in the shallower stops profile detailed in Table 3 above was not included in this study, due to the fact that the compartment pressures observed during decompression and at surfacing were not comparable with all other dives where shallower stops were used. The data obtained in this experiment will be briefly discussed later in the "*Case Study: Y – 40 Swimming Pool shallow decompression profile"* section.

Electrocardiographic Data

ECG records were obtained with superficial electrodes in a modified CM5 thoracic positioning. Data were collected with MP36 systems (Biopac Systems, Inc.), at a sampling rate of 1,000Hz, while the subjects were seated in a comfortable position.

There were two phases of continuous data collection: a 30-minutes pre-dive period used to establish the baseline condition for each volunteer and a 30-minutes post dive reading that was initiated 30 minutes after the end of the dive. This protocol was adopted due to previous observations that the magnitude of the changes in HRV tends to be higher in the second

half-hour post decompression [36]. Interestingly, it is well documented that venous gas bubbles counts tend to take approximately the same amount of time to reach a peak.
ECG recordings were converted into R-R normal-to-normal (as previously mentioned, the intervals between adjacent QRS complexes resulting from sinus node depolarizations) intervals. Each of these time-series was, then, subdivided into non-overlapping windows of 256 consecutive R-R intervals. Subsequently, the following estimators of HRV were obtained from each R-R window.

Time domain:

- R–R interval (heartrate).
- SDNN. Standard deviation of the normal-to-normal R-R interval, reflects all cyclic components acting on the cardiac variability, representing the joint action of the parasympathetic and sympathetic systems.
- RMSSD. The square root of the mean squared differences of successive R-R intervals, it is highly sensitive to short-term fluctuations and it is considered to reflect the parasympathetic activity.

Frequency domain: Fourier Discrete Transform, given by the equation below:

$$X(k) = \sum_{n=0}^{N-1} x(n) e^{-i w n}, \; where: \qquad \text{(eq 1)}$$

$$w = \frac{2\pi}{N} k$$

$$i^2 = -1$$

$$k = 0, \ldots, N-1$$

was performed, through the application of the computational algorithm Fast Fourier Transform (FFT), to obtain the Power Spectrum Density (PSD) [38], which was subsequently divided in:

- Ultra-low Frequencies: 0.01 to 0.04 Hz, not relevant to this study, due to the relatively short ECG recording intervals.

- Low Frequencies: 0.04 to 0.15 Hz, considered to reflect the joint action of the sympathetic and the parasympathetic components, probably with higher influence of the sympathetic system. It is also related to the baroreceptors activity [40] and, probably, endothelial function [46].
- High Frequencies: 0.15 to 0.4 Hz, historically assumed to be an estimator of the parasympathetic activity. It is, however, highly correlated with SDNN, possibly indicating that it is a broader indicator of variability also influenced by the sympathetic activity.

The variance $\sigma^2(Y)$ of a time-series Y(t) and the total power of the spectrum in the frequency domain are equal for $t \to \infty$ as shown below, where t is time. Consider that Y(t) is the sum of *n* individual components $Y_k(t)$, and each of these components can be expressed as the sum of a cosine and a sine waves of radial velocity ω_k with amplitude A_k:

$$Y_k(t) = A_k\,[\cos(2\pi\omega_k t) + \sin(2\pi\omega_k t)] \qquad \text{(eq 2)}$$

Now, the variance of an Y_k component of the time series during one of its cycles is given by:

$$\sigma_k^2 = \frac{\sum_{j=1}^{m_k}(Y_k - \bar{Y}_k)^2}{m_k} \qquad \text{(eq 3)}$$

Where $\bar{Y}_k$ is the mean value of the k^{th} component. Since Y_k is continuous, m_k is the size of the interval for one cycle, that is, $m_k = 2\pi \;\forall$ k, and $\bar{Y}_k = 0 \;\forall$ k, as illustrated bellow:

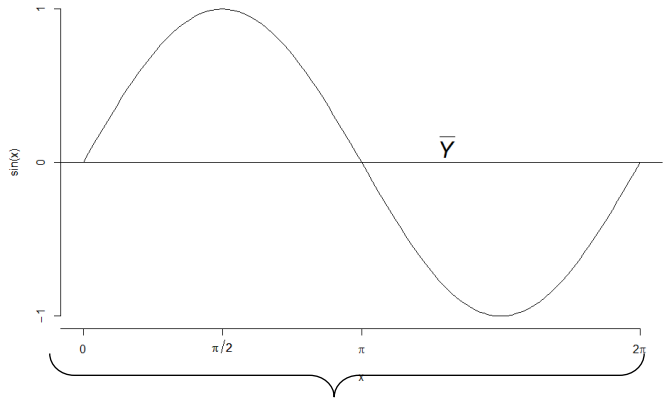

$$t' = w_k\, t$$

Once again, as Y_k is continuous, the summand in (4) is replaced by a definite integral. As explained above, the mean value is zero over a cycle, and therefore:

$$\sigma_k^2 = \frac{\int_0^{2\pi}[A_k\,(cos+sin)]^2}{2\pi} dt' \qquad \text{(eq 4)}$$

Where, for the sake of notation, we omit the product $2\pi\omega_k t$ in the sine and cosine functions. Developing (4) further, we have:

$$2\,\pi\sigma_k^2 = \int_0^{2\pi} A_k^2\,(sin^2 + cos^2 + 2\sin\cos)\, dt' \qquad \text{(eq 5)}$$

$$2\,\pi\sigma_k^2 = \int_0^{2\pi} A_k^2\,(sin^2 + cos^2) dt' + \int_0^{2\pi} A_k^2\; 2\cdot sin\cdot cos\, dt' \qquad \text{(eq 6)}$$

Since $(\sin^2 + \cos^2) = 1$ and the integral of the product sin · cos over a cycle is zero, we now have:

$$2\,\pi\sigma_k^2 = \int_0^{2\pi} A_k^2\, dt' = A_k^2\, 2\pi \qquad \text{(eq 7)}$$

Thus:

$\sigma_k^2 = A_k^2 \; \forall$ k (eq 8)

The total variance of the time-series is the sum of the n individual variances:

$\sigma_{Total}^2 = \sum_{k=1}^{n} A_k^2$ (eq 9)

Consider, now, the k component expressed in the frequency domain:

$F(\omega_k) = e^{z_k}$ (eq 10)

Where $z_k = \alpha_k + i \cdot \beta_k$. The power P_k of the k component in the spectrum is given by the product of z_k and its complex conjugate, $z^*_k = \alpha_k - i \cdot \beta_k$, so:

$P_k = (\alpha_k + i\beta_k)(\alpha_k - i\beta_k) = \alpha_k^2 + \beta_k^2 = R_k^2$ (eq 11)

Where R_k is the magnitude of the k^{th} component in the spectrum. The total power of the spectrum is the sum of the individual contributions. However, $R_k \equiv A_k$ and, therefore, the total power of the spectrum equals the variance of the time series, as given by equation 11.

In the present study, the power associated with a given PSD was approximated by $SDNN^2$, i.e., the square of the standard deviation of the R-R series. The shortcoming of such an approximation is that $R_k \equiv A_k$ is valid for $t \rightarrow \infty$, while the R-R series were limited to 256 values. The possible errors associated with that are discussed in a later section.

Low Frequencies and High Frequencies were also computed as fractions of the total power, as defined above (i.e., $SDNN^2$) and in normalized units (nu), where the respective frequency was divided by the sum of all calculated frequencies up to 0.4Hz. As an example, LFnu is equal to LF divided by the sum of ULF, VLF, LF and HF, multiplied by 100.

All data computational treatment was made through a set of implemented scripts in MatLab suite (MathWorks Inc.) and in R language.

Blood Samples

Venous blood was collected from an antecubital arm vein by a trained phlebotomist before and after each (simulated) dive. From each volunteer, four 5 ml tubes were obtained at each sampling. The first tube was used for the quantification of red cells, hemoglobin, hematocrit, neutrophils, lymphocytes, and platelets. The second tube was used to measure the concentrations of the enzymes aspartate transaminase (AST) and alanine transaminase, also referred to as alanine aminotransferase, (ALT) in the blood, thus controlling for liver function alterations due to decompression. The third and the fourth tubes were used for immunophenotyping and microparticles research through Flow Cytometry. These samples were collected using tubes Cyto-Chex BCT (Streck, INC).

Blood samples were drawn immediately before the experiment and one hour after the end of decompression. Blood works and liver function analyses were performed immediately after collection at the hyperbaric center. Immunophenotyping was performed up to 10 days after the blood collection (in the case of the experiments in Italy), although the average intervals between collection and analysis was 2 days (in all other cases).

Flow Cytometry

Immunophenotyping studies were performed with a 16-color FACSFortessa™ (Becton & Dickinson Company©, BD) using manufacturers' acquisition software.

Annexin binding buffer and the following antibodies were purchased from Biolegend (San Diego, CA): fluorescein isothiocyanate FITC-conjugated anti-annexin V, FITC-conjugated

anti-human myeloperoxidase (MPO), APC-conjugated anti-human CD41, PerCF594-conjugated anti-human CD14, PerCP-conjugated anti-human CD235, Pacific Blue-conjugated anti-human CD31, AF700-conjugated anti-human CD66b, and APC- conjugated anti-human CD19. Additionally, Live/Dead V-500 conjugated anti-human was used to define the dead cells population. Immunophenotyping through flow cytometry to evaluate the populations of granulocytes (CD 16+ / CD66b+) among live cells was performed, while controlling for the percentage of granulocytes expressing myeloperoxidase on its surface (MPO%) and mean fluorescence intensity of myeloperoxidase (MPO MFI), as indicators of neutrophil activation. The strategy used in this analysis and the hierarchy of the gates is detailed in Appendix I.

For MPs acquisition and processing, blood was centrifuged for 5 min at 1,500 g [47]. The supernatant was centrifuged at 15,000 g for 30 min to pellet the few remaining platelets and cell debris. These samples were then frozen at minus 80ºC, allowing all the samples to be analyzed on the same date. MPs were stained with Annexin V and analyzed as described in [11]. We define MPs as Annexin V-positive particles with diameters up to 1.0 µm. Gates were set to include from 0.3 µm to 1.0 µm particles, with exclusion of background corresponding to debris usually present in buffers. Detergent Triton X was used as a control, as MPs are expected to disappear in its presence.

Each sample analysis was performed using the software FlowJo Treestar© (FlowJo, Becton & Dickinson Company©, BD) at the Center for Experimental Research of the Hospital Albert Einstein.

Pulse Wave Amplitude calculated by Photoplethysmography

Pulse Wave Amplitude (PWA) measure by fingertip photoplethysmography (SS4LA transducer, BioPac Systems, Santa Barbara, CA) was used to estimate endothelial function. This technique was chosen due to the fact that it keeps strong correlation with ultra-sound based Flow Mediated Dilation (FMD) Index [48], a broadly used technique for endothelial

function assessment. Compared to conventional FMD, this method is low cost and does not require any special operator skills. Hence, it may be easily utilized as a screening tool in situations deprived of high-end ultrasound imaging devices and is not dependent on operator capabilities.

PWA was used to estimate changes in the endothelial function post decompression. Different studies have reported reduced endothelial function, measured as the vasodilation response (hyperaemia) driven by nitric oxide, following a transient period of provoked forearm ischemia [9] [49].

The protocol used was a combination of a 2-minute reading period, used to establish the baseline mean amplitude, followed by a 4-minute occlusion of the brachial artery through cuff inflation, followed by a 3-minute recording period. FMD Index was calculated as the ratio between the post-occlusion period mean wave amplitude, divided by the mean baseline wave amplitude, corrected by the non-occluded control arm, as described by [48] and detailed below:

$$FMD\ Index = \left(\frac{\frac{WA\ post\ ocl}{WA\ pre\ ocl}}{\frac{WA\ ca,\ \ post\ ocl}{WA\ ca,\ \ pre\ ocl}}\right), \text{ where:} \qquad \text{(eq 12)}$$

$WA\ post\ ocl = mean\ wave\ amplitude\ after\ occlusion$
$WA\ pre\ ocl = mean\ wave\ amplitude\ pre\ occlusion$
$WA\ ca, post\ ocl\ =\ mean\ wave\ amplitude\ of\ the\ contralateral\ arm\ after\ occlusion$
$WA\ ca, pre\ ocl = mean\ wave\ amplitude\ of\ the\ contralateral\ arm\ pre\ occlusion$

Each volunteer underwent two PWA measurements per trial, one immediately before the (simulated) dive and the second one hour after the experiment. To avoid interference caused by hand movement, all volunteers had their hands immobilized by splints during the experiment. An example of data recorded with the use of PWA is illustrated in the Figure 2 below.

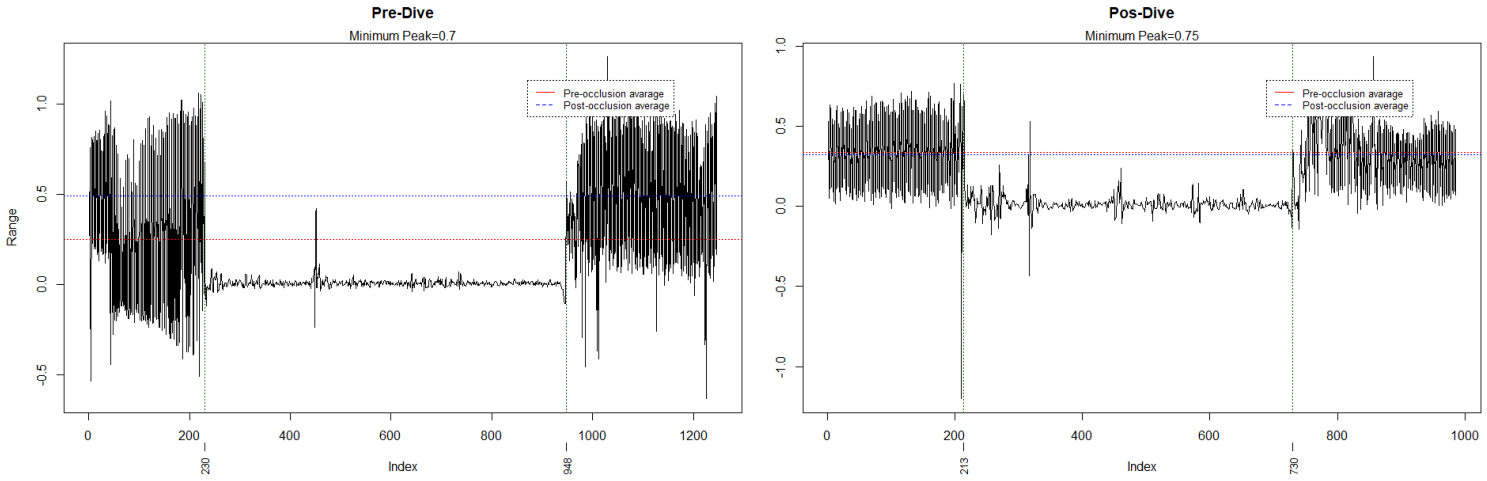

Figure 2. Illustrative PWA recording according to the protocol adopted. It is worth to note the difference in the average amplitude before and after occlusion, represented by the red and blue lines, respectively.

Decompression Schedules Determination

All decompression schedules were defined using ZHL-16b algorithm calculated through a script written in R language. Compartments half-times for nitrogen and helium were set to the original values published by Bühlmann A [50]. Maximum supersaturation pressures for each compartment at the end of the experiment were adjusted using Baker's gradient factors for each profile [51], calibrating the model to limit supersaturation for a factor of 0.85x for the Deeper Stops Profile and 0.65x for the Shallower Stops Profile. This calibration means that the intercept *a* of the linear equations used to limit the compartment *j* supersaturation for a given ambient pressure $P_{amb,}$ in the format $P_{\max j} = \frac{P_{amb}}{bj} + a_j$ were multiplied by 0.85 and 0.65, respectively.

Compartment on-gassing and off-gassing were calculated through the application of the following differential equation:

$$\frac{dP_j}{dt} = k_j \cdot \left(P_A - P_j\right) \qquad \text{(eq 13)}$$

Where P_j is the pressure of inert gas in compartment j, P_A is the alveolar (inspired) pressure of inert gas, and k_j is the inverse of the half-time of the compartment multiplied by the natural logarithm of 2 ($k_j = ln2 \cdot t_{\frac{1}{2}}^{-1}$). Solving (eq 13) we obtain:

$$P_j(t) = P_{0,j} \cdot e^{-k_j \cdot t} + P_A \cdot \left(1 - e^{-k_j \cdot t}\right) \qquad \text{(eq 14)}$$

Where $P_{0,j}$ is the initial pressure of inert gas in compartment j at the time of a change in the inspíred gas and/or hidrostatic pressure.

The typical gas absorption and elimination as modeled by this algorithm is illustrated in the Figure 3 below. This example was calculated using the parameters detailed in Table 1, Deeper Decompression Profile.

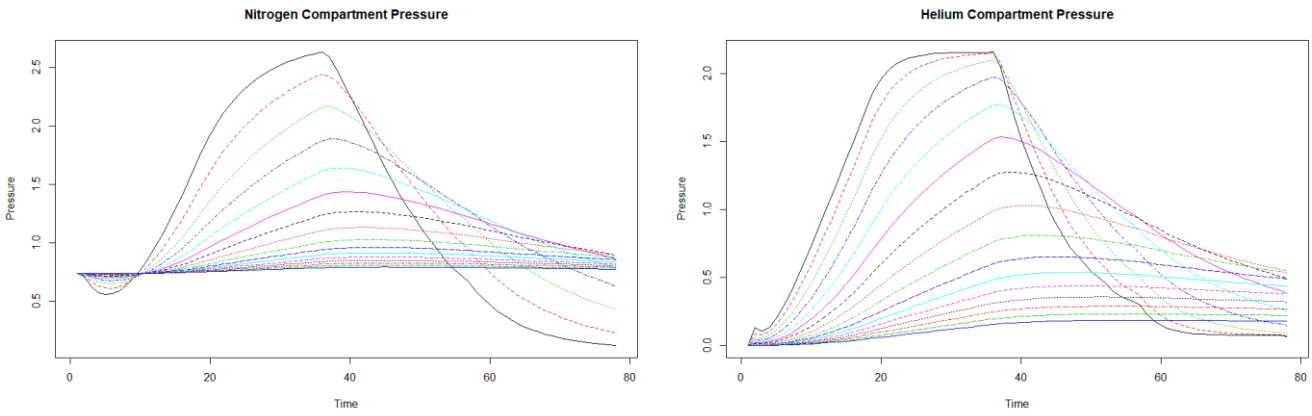

Figure 3. Estimated on / off-gassing by compartment according to ZHL-16b algorithm

Volunteers

Twenty-eight civilian and military divers participated in this study (one volunteer participated in two experimental rounds). Three volunteers participated in only one experiment, being released from the second due to medical conditions not related to dive (in two cases) and in one case due to the development of DCS in the first experiment. Blood samples for the quantification of red cells, hemoglobin, hematocrit, neutrophils, lymphocytes, platelets and for the assessment of liver function alterations (AST and ALT) were not obtained from all volunteers, therefore for each the result herein reported, the respective number of samples (*n*) will be reported. Table 4 below summarizes the anthropometric data of the study population. Data is given as the mean ± standard deviation (s.d.)

Table 4. *Study population characteristics*

Age (years)	43.6 ± 6.5
Weight (kg)	87 ± 12.4
Height (cm)	179 ± 7.9
BMI	26.9 ± 3.5

Distribution of the volunteers between the experimental facilities (Table 5).

Table 5. *Volunteers distribution per experimental facility*

Centro Hiperbárico Paulista	23
CIAMA	3
Y – 40 Swimming Pool	4

Statistical Analyzes

Differences between pre and post dive data were determined using two-sided Student's t test for paired samples for the cases where a normal distribution of the observations was verified. When normal distribution was not confirmed, a non-parametric permutation test

with 10.000 simulation rounds was performed for the definition of the p-value [52]. The limit of significance was set at 5%.

All data provided in this study is given as the mean ± standard error (S.E.)

Modeling

Modeling was done using a Radial Basis Function Neural Networks (RBF-NN), as detailed below, univariate and multivariate regressions. RBF-NN and multivariate were used in order to allow the comparison of the accuracy produced by each one and, since the RFB-NN provided a much higher accuracy, all the results obtained through multivariate regression were discarded and will not be discussed in this paper. The dataset was structured as a matrix *G'* composed by elements $x'_{k,h}$, where:
h represents the h^{th} variable (h = 1, 2,…, n),
k represents the k^{th} volunteer (k = 1, 2,…, N)
n is equal to the number of observed variables
N is equal to the number of volunteers.

Data was treated so that all variables were normalized according to equation 15 below and used to create the normalized matrix G:

$$x_{k,h} = \frac{x'_{k,h} - \min(x'_h)}{max\,(x'_h) - \min(x'_h)} \quad \text{, where:} \quad \text{(eq 15)}$$

$x_{k,h} = the\ normalized\ variable$

$$G = \begin{bmatrix} x_{11} & x_{12} & \cdots & x_{1n} \\ x_{21} & x_{22} & \vdots & \vdots \\ x_{31} & x_{32} & x_{k,h} & \\ \vdots & \vdots & & \\ x_{N1} & x_{N2} & & x_{Nn} \end{bmatrix}$$

RBF-NN was structured as the function Ψ, given by the sum of Gaussian radial basis functions:

$\Psi = \sum_{j=1}^{S} a_j \, \gamma_j + b$, where: (eq 16)

a_j $= calculated\ coefficient\ for\ number\ of\ clusters\ j$

b $= adjustment\ coefficient$

Where γ_j is given by:

$\gamma_j(x) = e^{-1/2\sigma^2 \| x_{N1}, x_{N2}, \ldots, x_{Nn} - M_j \|^2}$, where: (eq 17)

j $= number\ of\ clusters, where\ j = 1, 2, \ldots, S$

$M_j = centroids\ for\ any\ given\ cluster. M_j$

$= [m_{1,j}, m_{2,j}, m_{3,j}, \ldots, m_{n,j}], thus:$

$M_j = \{m_{h,j}\}$

The centroids vector M_j were stochastically determined between [0, 1]. The Euclidean distance $E_{k,j}$, given by the sum of the norms $\| x_{k,h} - M_j \|^2$, is equal to:

$E_{k,j} = \sum_{h=1}^{n} (x_{k.h} - m_{h,j})^2$ (eq 18)

For the model used in this study one single sigma was calculated for all centroids, as per equation 19 below. The utilization of one sigma for each centroid might improve the accuracy of the model in certain cases [53], but did not add additional accuracy in this case.

$\sigma = \frac{D_{max}}{\sqrt[2]{2S}}$, where: (eq 19)

Dmax = maximum distance between any pair of centroids

S = number of centroids

The calculated coefficients $a_{1,}a_2, \ldots, a_j$ and the adjustment coefficient b, used to construct the matrix *w*, were determined by solving the system below:

$$\underbrace{\begin{bmatrix} e^{-\frac{E_{k,j}}{2\sigma^2}} & \cdots & e^{-\frac{E_{k,j}}{2\sigma^2}} & 1 \\ \vdots & \ddots & \vdots & \vdots \\ e^{-\frac{E_{k,j}}{2\sigma^2}} & \cdots & e^{-\frac{E_{k,j}}{2\sigma^2}} & 1 \end{bmatrix}}_{\Theta} \cdot \underbrace{\begin{bmatrix} a_1 \\ a_2 \\ \vdots \\ a_j \\ b \end{bmatrix}}_{w} = \underbrace{\begin{bmatrix} y_1 \\ y_2 \\ \\ \vdots \\ y_N \end{bmatrix}}_{y}$$

Since Θ is a not a square matrix, the pseudo-inverse matrix Θ^{-1} was calculated, as follows:

$$\Theta^{-1} = (\Theta^t . \Theta)^{-1} . \Theta^t \qquad \text{(eq 20)}$$

Θ^t is the transpose of Θ.

Therefore:

$$w = \Theta^{-1} . \ y \qquad \text{(eq 21)}$$

A total of 10.000 iterations is made for the calculation of the coefficients a_j and b_j and the set $\{a_j , b_j\}$ that provides the highest accuracy in the training set is chosen for the model. It is important to note that the number of iterations was arbitrarily defined.

The optimal number of clusters was determined using K-means algorithm, calculated for each set of training data, given by the minimization of the distance *J*, given by:

$J = \sum_{i=1}^{k} \sum_{j=1}^{S} \left\| x_{k,h} - M_j \right\|^2$, where: (eq 22)

In order to reduce the arbitrariness usually associated with the determination of the number of clusters that will be used in construction of the RBF-NN, a decay curve approximation of the sum of the within cluster sum of distances (WS) was created, according to the formula below:

$WS_n = WS_1 * j^{-\varepsilon}$, where: (eq 23)

$WS_n = sum\ of\ within\ distance\ for\ the\ n\ number\ of\ clusters$

$\varepsilon = calculted\ decay\ coefficient$

ε is calculated according to the linearized form of equation 23.

$\log(WS_j) = \log WS_1 - \varepsilon * \log(j)$ (eq 24)

For the purposes of the later discussion, the accuracy of the model was defined as the Root Mean Squared Error (RMSE) of the predicted versus the observed SDNN Ratio.

SDNN Ratio is calculated as the SDNN measured after the experiment divided by the SDNN measured before the experiment.

Due to the relatively small sample, two different models were created. In the first model, the RBF-NN was trained with the data obtained in both profiles from all volunteers (*N* = 47), with the objective of finding out whether a relationship between the SDNN Ratio and the ratios of the observed variables (CD16(%), CD66b (MFI), MPO(%), MPO (MFI), Anexxin +, MP CD66b +, MP CD31+ and MP CD41+ calculated as the post experiment

values divided by the pre experiment values). For clarification purposes, training the RBF-NN means creating a matrix *G*, with *N* equal to 47 (all the volunteers available), and *n* equal to 7 (the variables mentioned above).

A second model was created, where the calibration of the RBF-NN was done using only a portion of the data ($N = 37$), chosen in a stochastic process. As in the first model, Gaussian functions were chosen for activation and the model was based on the neural network that produced the best accuracy for the training set in 100 trials, in a stochastic process of centroids determination. The model created was then applied to the remaining 10 observations in an out-of-sample validation process. Additionally, a Principal Component Analysis was performed, using eigenvalue decomposition of data covariance, in order to explore the largest possible variance of the data explained by each principal component [54].

Results

Overall, volunteers reported no adverse effects from any of the experiments. There was only one case of decompression sickness diagnosed after a Deeper Decompression Profile in the Navy facility, which was promptly treated according to the parameters of the US Navy Recompression Treatment Table 4 by the facility physician, with complete recovery immediately after treatment.

Cluster analysis

With the objective of analyzing the overall behavior of the dataset and evaluate whether there were differences caused by the experimental profiles, a cluster analysis was performed. The clustering problem is defined as the problem of finding homogeneous groups of data points in a given data set, or, in other words, as subgroups where the distance between its elements and an arbitrary centroid can be calculated as a function of the number of subgroups. Each of these groups is called a cluster and can be defined as a region in which the density of objects is locally higher than in other regions [55].

The first step was to assess in how many clusters the dataset could be split, based on the minimization of the within cluster sum of distances variation, as described in the Material and Methods session.

Figure 4 displays a plot of the within cluster sum of distances variation as function of the number of clusters was made for each experimental profile.

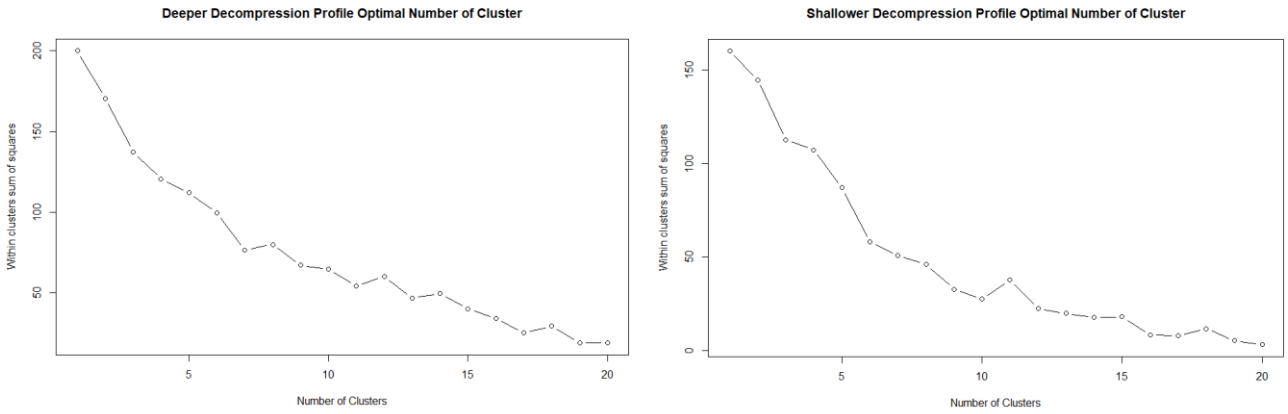

Figure 4. Sum of within clusters distance variation according to the number of clusters.

A visual inspection of the plots indicates that an increase in numbers of clusters after approximately the 10th cluster, in the case of the Deeper Decompression Profile, has little impact in the overall sum of within distances, demonstrating that the dataset can be divided in approximately 10 subgroups. Although the plot for the shallower profile is not substantially different, there is a steeper decrease in the within cluster sum of distances before the 5th cluster, indicating that the dataset might probably be divided in a smaller number of subgroups.

This partitioning method has limitations, due to the usually arbitrary definition of the ideal number of clusters, however it brings important insights about patterns that might be formed in the dataset.

The second technique used to reduce the arbitrariness of the previous method was the Principal Components Analysis (PCA). Table 6 below displays the PCA results. Although the relative variance explained by principal component number 1 is higher for the Deeper Decompression Profile, the cumulative variance explained by the first four components is higher than 75% in both experimental profiles.

Note: before the PCA analysis was made, the dataset was normalized by the standard deviation, according to the equation 25 below:

$$y = \frac{(x_k - \bar{x})}{\sigma_x}$$, where: (eq 25)

$y = the\ normalized\ variable$

$\bar{x} = \frac{1}{N} \sum_{k=1}^{N} x_k$

$\sigma_x = \sqrt{\sum (x_k - \bar{x})^2}$

Figure 5 illustrates the cumulative variance as function of the number of principal components taken into consideration. For further reference, Appendix II contains the detailed composition of each principal component.

Table 6. *Principal Component Analysis*

	Shallower Decompression Profile							
	PC1	PC2	PC3	PC4	PC5	PC6	PC7	PC8
Proportion of Variance	0,25	0,23	0,18	0,13	0,10	0,07	0,04	0,01
Cumulative Proportion	0,25	0,48	0,66	0,79	0,89	0,96	0,99	1,00
	Deeper Decompression Profile							
	PC1	PC2	PC3	PC4	PC5	PC6	PC7	PC8
Proportion of Variance	0,33	0,18	0,14	0,11	0,10	0,08	0,04	0,03
Cumulative Proportion	0,33	0,50	0,64	0,75	0,85	0,93	0,97	1,00

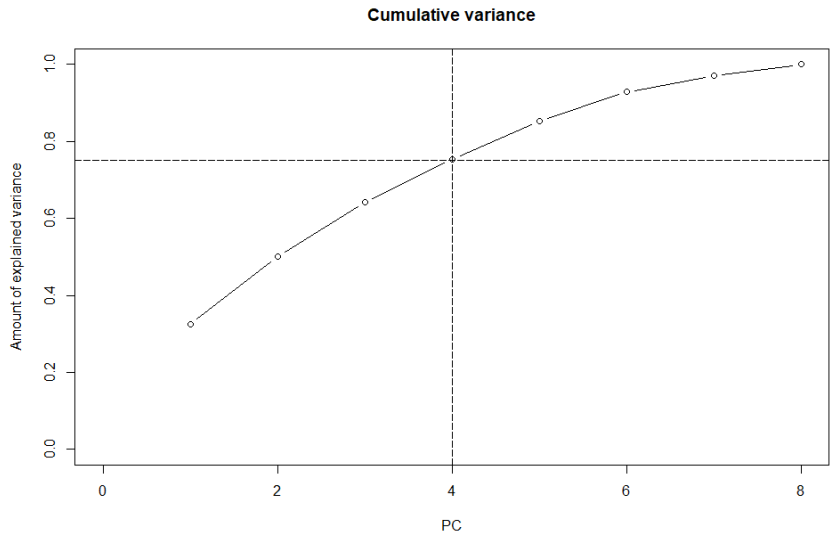

Figure 5. Amount of variance explained by each PC, as reported in Table 6

Finally, the volunteers were divided in 4 clusters (calculated according to the within cluster sum of distances, as defined in equation 21) since, as observed above, the first 4 principal components explain more than 75% of the variance in either case and plotted against the influence of each of the two principal components for each data point (Figure 6).

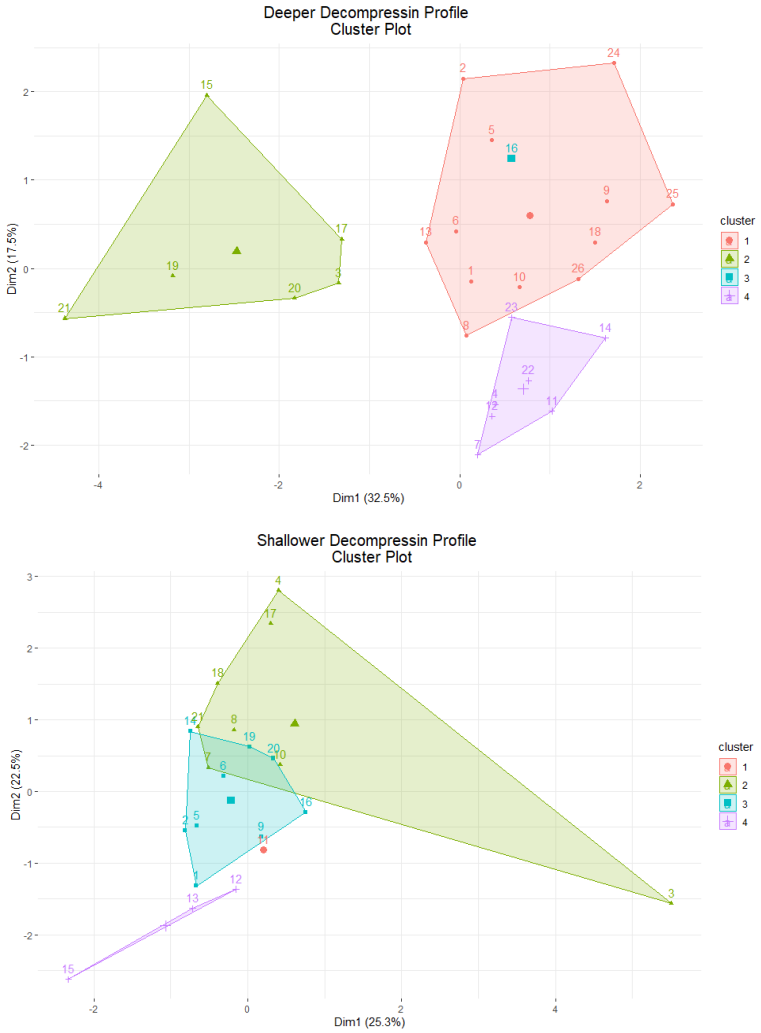

Figure 6. Volunteers distribution within 4 clusters for each experimental profile

As illustrated in the cluster classification above, data points representing volunteers were grouped in different areas of the chart depending on the decompression profile to which they were exposed. It becomes clear that the results obtained from the two different decompression profiles show important differences in many of the variables analyzed and

the respective response by the volunteers. Due to this fact, the results will be divided between Deeper Decompression and Shallower Decompression Profiles and presented accordingly. When not divided according to the experimental profile, results will be divided between pre dive and post dive values.

Heart Rate Variability

HRV was evaluated for all volunteers in both, time and frequency domains. An overall increase in variability was observed in all situations.

In the experiments where Deeper Decompression Profiles were used, the frequency domain indicators LF, Total Low Frequencies (VLF + LF) and HF increased, but only the two latter showed significant increases. LF as proportion of HF and as proportion of total variability did not show significant changes, neither did HF as proportion of total variability. SDNN and RMSSD, in the time domain, the post dive values showed significant increases (Table 7).

Table 7. *Heart Rate Variability - Deeper Decompression Profile*

	pre dive mean	SE	post dive mean	SE	p-value
Low Frequency (ms^2)	429,87	61,31	551,11	77,91	0,058
Total Low Frequencies (ms^2)	773,88	78,72	1098,48	111,32	0,047
High Frequency (ms^2)	75,46	13,21	188,48	26,87	0,045
LF / HF Ratio	8,60	1,29	8,76	1,54	0,234
LF as ratio of Total Variability	0,21	0,02	0,23	0,02	0,117
Total Low Frequencies as ratio of Total Variability	0,29	0,02	0,23	0,02	0,097
High Frequency as ratio of Total Variability	0,03	0,00	0,04	0,00	0,077
RMSSD	20,46	1,50	25,31	2,45	0,024
SDNN (ms)	43,71	2,21	47,52	3,61	0,094

The Shallower Decompression Profiles also provoked an overall variability increase. In the frequency domain, HF showed significant increases. In the time domain SDNN and RMSSD post dive values showed significant increases. LF as proportion of HF and as proportion of total variability did not show significant changes, neither did HF as proportion of total variability (Table 8).

Table 8. *Heart Rate Variability- Shallower Decompression Profile*

	pre dive mean	SE	post dive mean	SE	p-value
Low Frequency (ms^2)	478,42	65,00	647,35	127,12	0,066
Total Low Frequencies (ms^2)	774,48	85,49	820,71	163,55	0,053
High Frequency (ms^2)	61,54	9,01	94,45	18,64	0,034
LF / HF Ratio	9,20	1,01	9,68	1,37	0,195
LF as ratio of Total Variability	0,25	0,03	0,23	0,03	0,129
Total Low Frequencies as ratio of Total Variability	0,33	0,03	0,31	0,03	0,165
High Frequency as ratio of Total Variability	0,03	0,00	0,03	0,01	0,076
RMSSD	19,30	1,37	25,42	3,04	0,019
SDNN (ms)	42,91	2,25	49,48	3,82	0,035

Shallower Decompression Profiles caused a higher increase in post dive variability, given by SDNN (42.9 ± 2.25 to 49.5 ± 3.82, p-value = 0.037), than Deeper Decompression Profiles (43.7 ± 2.21 to 47.5 ± 3.61, p-value = 0.09, Figure 7). The same kind of variation was observed in the RMSSD index. Both profiles caused significant changes in the RMSSD index, with the Shallower Decompression Profile causing an increase from 19.3 ± 1.37 to 25.4 ± 3.04, p-value = 0.018, and the Deeper Decompression Profile increasing the index from 20.4 ± 1.5 to 25.3 ± 2.45, p-value = 0.024 (Figure 7).

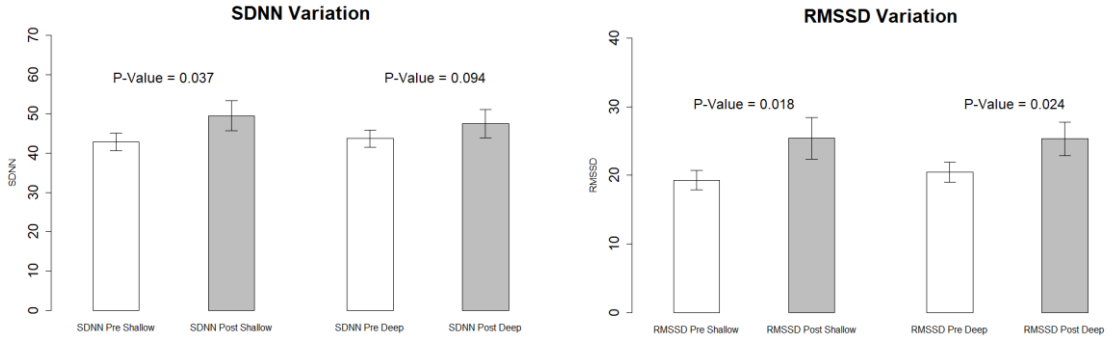

Figure 7. mean SDNN and RMSSD pre and post dive for each decompression profile

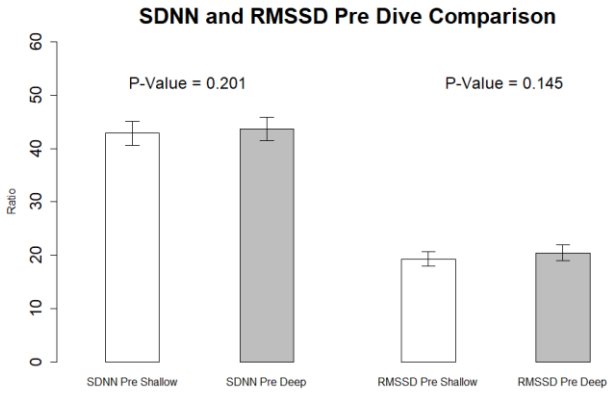

Figure 8. SDNN and RMSSD pre dive values comparison

Both, the baseline SDNN and RMSSD values did not present statistically different means between the profiles, as demonstrated in Figure 8.

Additionally, there was noticeable difference between the number of volunteers that had a reduction in the SDNN in each profile. The Deeper Stops Profile was associated with a decrease in the SDNN in 30% of the volunteers (8 out of 26), while in Shallower Stops Profile 21% of the volunteers (5 out of 23) showed a reduction in this indicator (Figure 9)

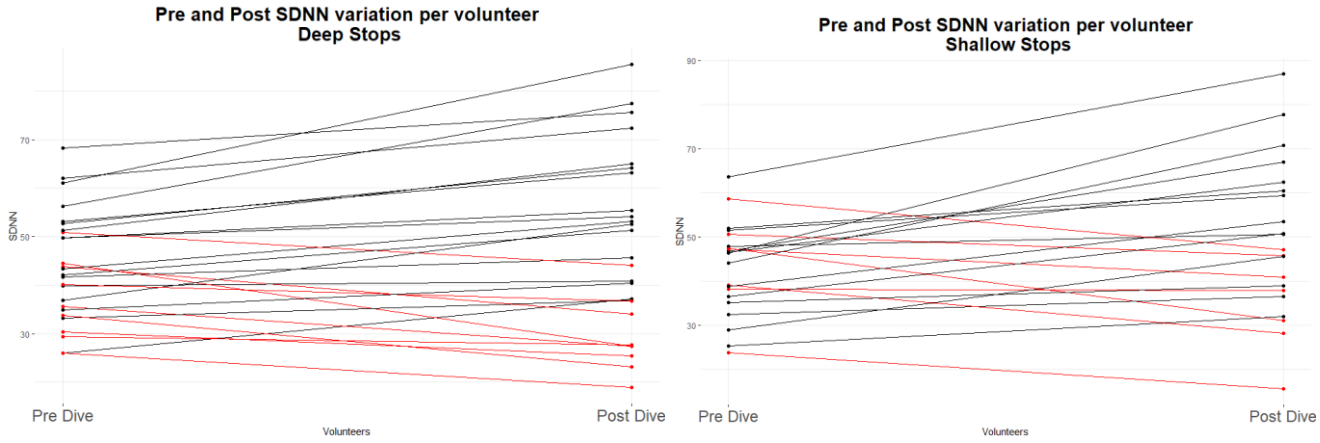

Figure 9. Illustration of the SDNN changes observed in the volunteers in each decompression profile. The red lines represent the volunteers for which the post dive SDNN values were lower than the pre dive values.

All the five cases where SDNN was lower after the dive with the Shallower Stops Profile also presented a reduction in the SDNN when the dive was executed with the Deeper Stops Profile. In other words, the 8 volunteers whose SDNN decreased in the Deeper Stops Profile comprise all the 5 ones that presented the same behavior in the Shallower Stops Profile.

Pulse Wave Amplitude and FMD Index

The vast majority of the volunteers presented a reduction in the PWA post occlusion in the post dive observation. While the pre dive PWA values are not significantly different between the profiles, the post dive values for the Deeper Decompression Profile are significantly lower than values observed in the Shallower decompression Profile, as illustrated in Figure 10.

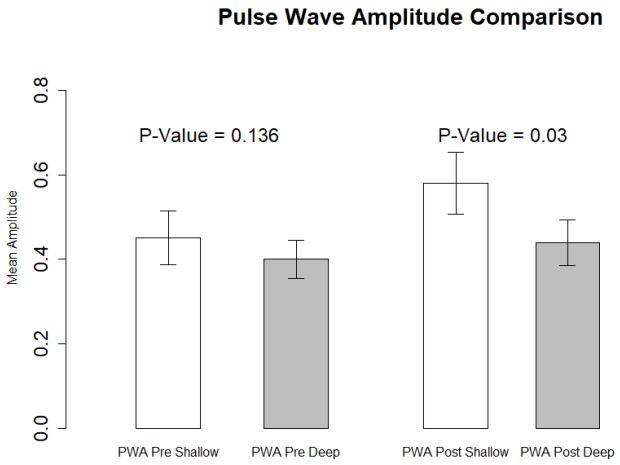

Figure 10. Average mean Pulse Wave Amplitude measured before and after the simulated dive for each decompression profile. It can be noted that, although the pre dive means are not statically different, the post dive values differ according to the decompression profile used.

Interestingly, most of the cases where there was an increase in the FMD index, it was due to a large reduction in the pre occlusion measurement, combined with a maintenance or

lesser reduction of the post occlusion PWA, suggesting a baseline vasoconstriction post dive. However, it is important to note that fingertip photoplethysmography is not an adequate method to measure vasoconstriction or vasodilation for the same individual in different moments, due to the fact that the removal and repositioning of the probe between readings might affect the observed result and cause them not to be necessarily comparable.

The FMD index (equation 12) variation per volunteer, according to the experimental profile, is displayed in Figure 11, below.

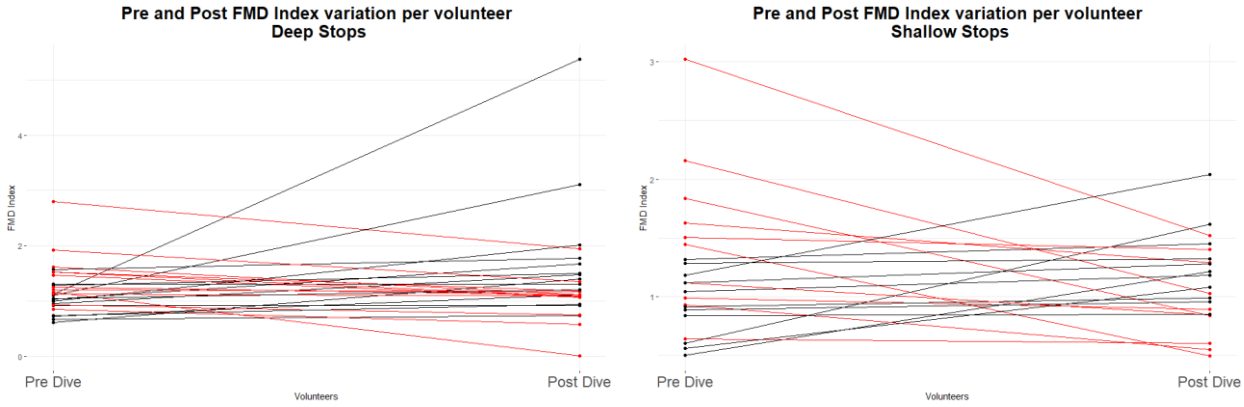

Figure 11. Illustration of the FMD Index changes observed in the volunteers in each decompression profile. The red lines represent the volunteers for which the post dive FMD indexes were lower than the pre dive FMD indexes. It is important to note that, in the Deeper Decompression Profile, there were two volunteers that presented a markedly decrease in the post dive pre occlusion PWA, causing the FMD Index to disproportionally increase, not due to compensatory hyperemia response to occlusion, but due to the large reduction in the index denominator.

If the two outliers clearly observed in Figure 11, Deep Stops Profile, are removed from the analysis, the average FMD Index for both profiles would not be statically different, as observed in Figure 12. This exercise is interesting to exclude the effects of large reduction in the index denominator either due to vasoconstriction or reading error.

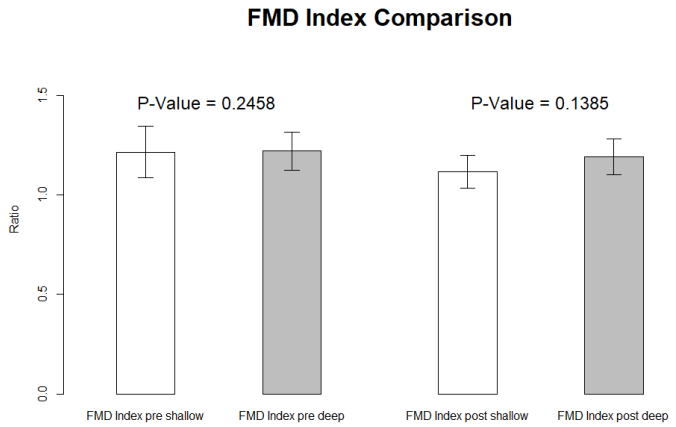

Figure 12. Pre and post FMD Index comparison for both profiles. It can be observed that the pre and post average values are not different between the decompression profiles.

***Blood Assay*.**

Blood assays were performed for 25 volunteers. Leucocytes, red blood cells, hematocrit, hemoglobin and platelets counts were different between pre and post dive measurements. Significant reductions in red blood cells, hematocrits, hemoglobin and platelets were observed, concomitantly with increases in leucocytes counts. Table 9 details the changes observed in the Deeper Decompression Profiles, and Table 10 brings the observed values for the Shallower Decompression Profiles. A comparison between the pre and post dive results collected from both profiles was made, resulting in the conclusion that pre dive data was similar (p-value > 0.5 for all blood assay indicators evaluated) and that data collected post dive was also similar (p-value > 0.5) for both profiles. It means that the type of alteration produced by the dives was approximately the same, with slightly different intensities, depending on the profile (Figure 13).

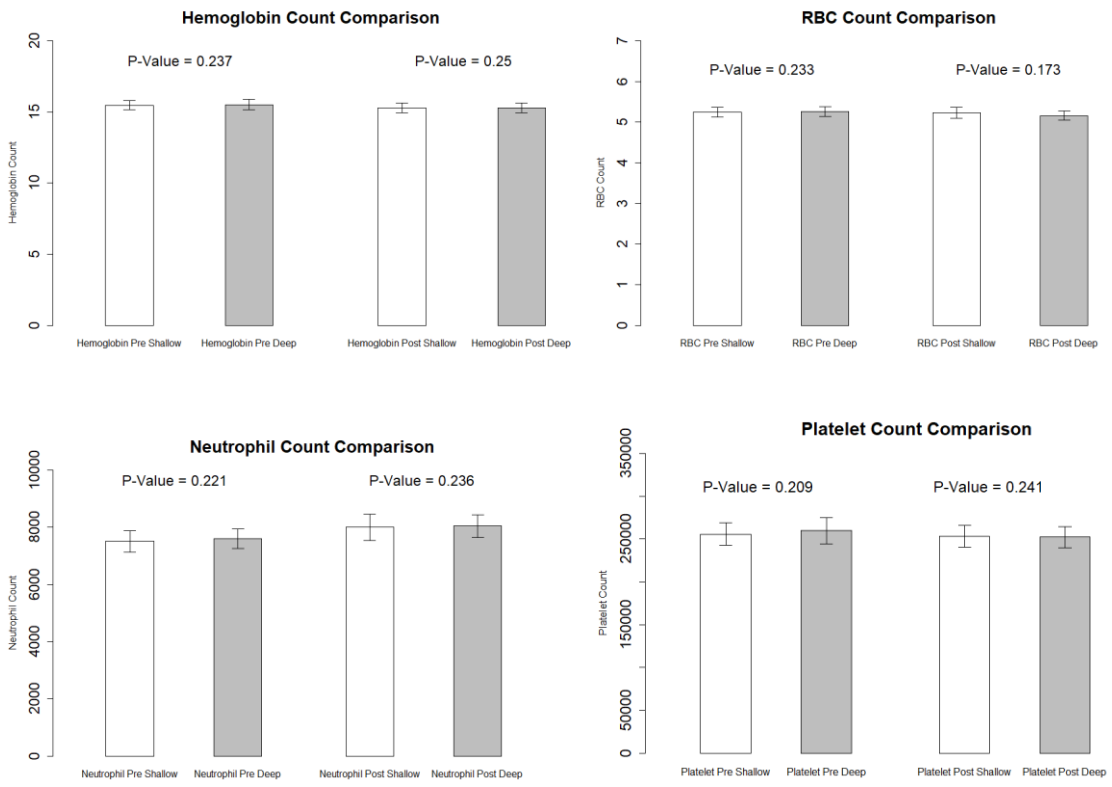

Figure 13. Pre and Post dive results for both dive profiles. As it can be noted, the baseline values and the Post dive results are not statically different among each other.

Liver function

Enzymes aspartate transaminase (AST) and alanine transaminase, also referred to as alanine aminotransferase (ALT) were measured pre and post dive for 12 volunteers (n=12), in order to control for liver function alterations due to decompression. No significant changes were observed in either case, as detailed in tables 9 and 10.

Table 9. *Red cells, hematrocit, leukocyte, platelet counts and liver fuction indicators - Deeper Decompression Profile*

	pre dive mean	SE	post dive mean	SE	p-value
WBC x 10^3	7,59	0,34	8,04	0,39	0,085
Platelets x 10^5	2,60	0,15	2,52	0,13	0,040
Red Cells (abs)	5,26	0,0001	5,16	0,11	0,015
Hemoglobin (abs)	15,52	0,0004	15,29	0,35	0,006
Hematocrit (abs)	44,88	0,0010	44,09	0,60	0,083
AST	19,38	2,18	20,46	1,72	0,237
ALT	34,38	6,24	33,92	6,13	0,636

Table 10. *Red cells, hematrocit, leukocyte, platelet counts and liver fuction indicators - Shallower Decompression Profile*

	pre dive mean	SE	post dive mean	SE	p-value
WBC x 10^3	7,51	0,38	8,00	0,46	0,008
Platelets x 10^5	2,56	0,14	2,53	0,13	0,197
Red Cells (abs)	5,25	0,0001	5,23	0,14	0,342
Hemoglobin (abs)	15,48	0,0003	15,29	0,35	0,046
Hematocrit (abs)	45,13	0,0010	44,92	0,73	0,284
AST	24,85	3,80	25,46	4,35	0,450
ALT	42,31	10,81	43,54	10,81	0,270

Flow Cytometry

Immunophenotyping through flow cytometry to evaluate the populations of granulocytes (CD 16+ / CD66b+) among live cells was performed, while accounting for the percentage of granulocytes expressing myeloperoxidase on its surface (MPO%) and the mean fluorescence intensity of myeloperoxidase (MPO MFI), as indicators of neutrophil activation [56]. While the Deeper Decompression Profile (Table 11) caused an increase in all the variables observed (except for a non-significant reduction in the percentage of cells expressing MPO), the Shallower Decompression Profile caused a discrete increase in the total granulocytes, but a reduction in circulating neutrophils, MPO expression and the percentage of cells expressing MPO (Table 12).

Table 11. *Granulocytes, neutrophils and MPO - Deeper Decompression Profile*

	pre dive mean	SE	post dive mean	SE	p-value
CD16+	11,36	2,13	13,29	2,08	0,01
CD66b (MFI)	499,90	52,38	544,55	65,81	0,33
MPO + (%)	2,45	0,83	2,55	0,89	0,76
MPO (MFI)	576,80	171,40	526,57	137,53	0,47

Table 12. *Granulocytes, neutrophils and MPO - Shallower Decompression Profile*

	pre dive mean	SE	post dive mean	SE	p-value
CD16+	12,19	1,79	13,51	1,85	0,28
CD66b (MFI)	587,47	37,91	572,07	37,69	0,38
MPO + (%)	2,61	1,17	2,32	1,16	0,15
MPO (MFI)	314,95	31,93	291,05	28,29	0,07

MPs were assessed by Annexin V staining and discriminated by CD31, CD41 and CD66b markers to differentiate MPs derived from endothelial cells, platelets and granulocytes, respectively. The population of MPs was defined as positive for Annexin and analyzed as previously described, using microbeads with diameters of 0.3 µm and 1.0 µm to carefully assess the size of particles. Number of MPs were observed and, as in most of the results reported in this study, there were important differences between the values observed with different decompression profiles. Table 13 displays the MP counting for Deeper Decompression Profile, where a significant increase was observed in the CD31+ and CD41+ populations. An increase in the values of Annexin + and a decrease in CD66b MPs count were not significant.

Table 13. *Microparticules - Deeper Decompression Profile*

	pre dive mean	SE	post dive mean	SE	p-value
Annexin +	3,85	0,51	4,13	0,61	0,182
CD66b+	0,23	0,06	0,21	0,05	0,207
CD31+	0,06	0,02	0,17	0,06	0,022
CD41+	24,52	4,59	35,77	5,16	0,027

The Shallower Stops Profile caused a significant increase in CD66+ MPs. A reduction in CD31+ MPs and an increase in CD41+ MPs was not significant (Table 14).

Table 14. *Microparticules - Shallower Decompression Profile*

	pre dive mean	SE	post dive mean	SE	p-value
Annexin +	3,62	0,51	3,57	0,44	0,232
CD66b+	0,21	0,04	0,40	0,12	0,025
CD31+	0,35	0,21	0,16	0,08	0,121
CD41+	49,80	6,80	53,46	6,96	0,176

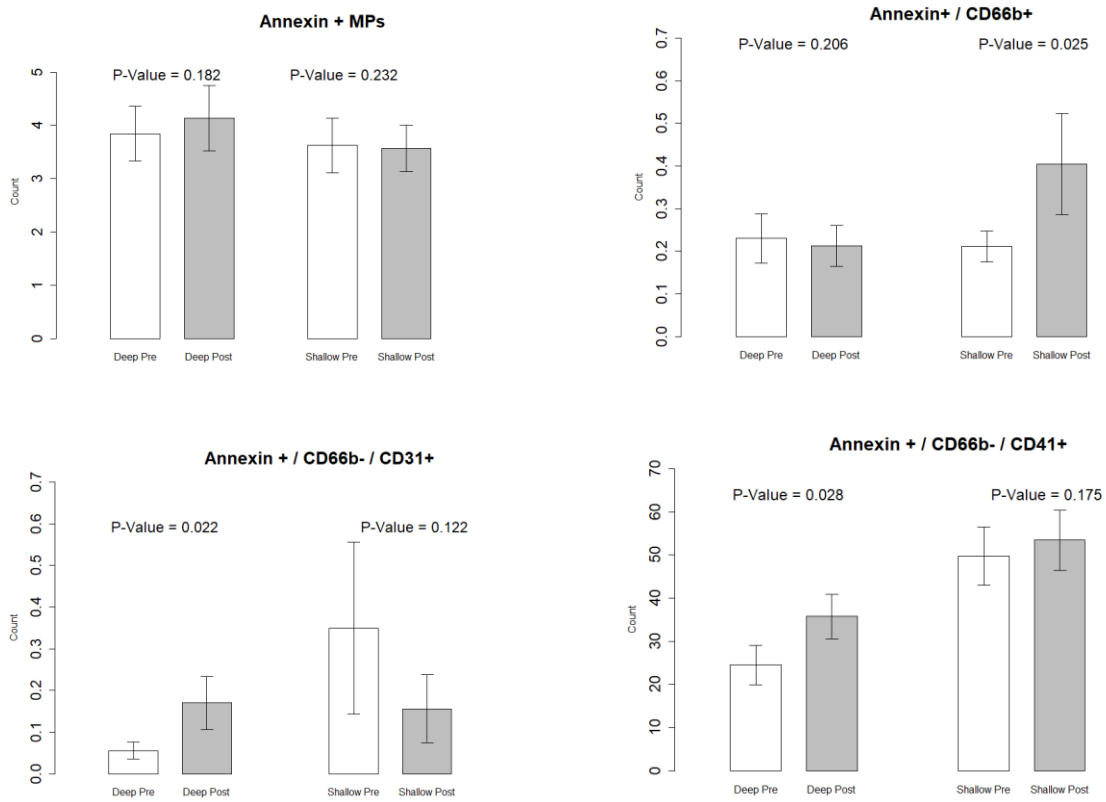

Figure 14. Pre and Post MPs count for each decompression profile. Deeper Decompression Profile is simply referred to as “Deep” and the Shallow Decompression Profile is referred to as “Shallow”. Important to note that this test was not paired.

Linear Regressions

Univariate regressions (n = 47) between SDNN, LF, HF and FMD Index, and immune system action markers obtained through flow cytometry were calculated before (Table 15) and after the dive (Table 16) and the coefficient (estimate) and p-values were extracted for each one.

Table 15. *Relationship betweem HRV, FMD, Immune System Activation Markers and MPs - Pre dive model*

	SDNN		LF		HF		FMD	
	Estimate	p-value	Estimate	p-value	Estimate	p-value	Estimate	p-value
CD16 +	-22,89	0,09	-5,11	0,24	-0,94	0,25	0,0014	0,85
CD66b MFI	-0,55	0,28	-0,03	0,89	-0,05	0,16	0,0004	0,28
MPO (%)	-2,68	0,91	1,08	0,89	-1,66	0,25	-0,0151	0,24
MPO (MFI)	0,44	0,01	0,07	0,23	0,01	0,28	-0,0001	0,43
Annexin +	-125,37	0,03	-25,45	0,16	-7,70	0,02	-0,0196	0,53
CD66b +	195,27	0,74	376,92	0,04	34,12	0,33	0,1455	0,65
CD31 +	78,87	0,72	122,34	0,08	2,00	0,88	-0,0465	0,70
CD41 +	3,14	0,52	1,83	0,23	0,09	0,74	0,0006	0,82

Table 16. *Relationship betweem HRV, FMD, Immune System Activation Markers and MPs - Post dive model*

	SDNN		LF		HF		FMD	
	Estimate	p-value	Estimate	p-value	Estimate	p-value	Estimate	p-value
CD16 +	-37,17	0,18	-11,70	0,11	-1,98	0,25	-0,00496	0,67
CD66b MFI	-0,76	0,43	-0,25	0,38	-0,06	0,25	0,00003	0,43
MPO (%)	-42,94	0,34	-12,56	0,30	-2,21	0,43	0,02467	0,19
MPO (MFI)	0,70	0,09	0,09	0,45	0,05	0,08	0,00030	0,08
Annexin +	-238,91	0,02	-52,04	0,06	-9,96	0,12	-0,07949	0,05
CD66b +	796,83	0,23	302,16	0,09	17,84	0,67	-0,01505	0,96
CD31 +	-444,86	0,58	-185,78	0,39	-7,09	0,89	0,39148	0,25
CD41 +	5,85	0,53	3,33	0,18	0,12	0,83	0,00059	0,88

It can be observed in Table 15 that SDNN and the FMD Index showed significant negative correlations with number of circulating Annexin+ MPs. The Lower Frequencies of the spectrogram have a higher positive association with CD66b+ and CD31+ MPs, although not statically significant for the second.

Linear regressions between HRV indicators and FMD Index are detailed in Table 17. There were positive significant correlations between the FMD Index, and the natural logarithm of Higher Frequencies normalized units, RMSSD and SDNN. There was no significant correlation between the natural logarithm of Lower Frequencies normalized units and the FMD Index.

In order to explore how the FMD Index would correlate with changes in the sympathovagal balance, two ratios were calculated: (i) the natural logarithm of the ratio of Lower Frequencies by Higher Frequencies and (ii) the natural logarithm of Lower Frequencies Ratio, divided by the Higher Frequencies Ratio, called herein Frequency Variation Ratio

(FPR) as defined in equation. In both cases there were no significant inverse correlations between the calculated ratios and the FMD Index.

$$FPR = \ln\left(\frac{\frac{LF\ post}{LF\ pre}}{\frac{HF\ post}{HF\ pre}}\right) \quad \text{(eq 26)}$$

Table 17. *Relationship betweem FMD Index and Heart Rate*

	Estimate	p-value
LN - HF nu	8,0596091	0,04
LN - LF nu	0,5977665	0,62
LN - LF / HF	-0,2061642	0,29
LN - FPR	-0,7767077	0,25
RMSSD	0,4122662	0,05
SDNN	0,2983776	0,04

A correlation test between HFnu and LFnu and the alternative normalization method (described in the Materials and Methods), where total variance is approximated by $SDNN^2$ was performed. As expected, there are positive significant correlations between HFnu and HF divided by $SDNN^2$, and LFnu and LF divided by $SDNN^2$ (0.70 and 0.73, respectively, p-values < 0.0001).

A correlation coefficient between all variables, and its respective *p-value*, was calculated (Table 18). These coefficients were calculated for the data set for which all variables of interest were collected (n = 37), therefore the data displayed in Table 18 is not necessarily comparable to the data displayed in Tables 15, 16 and 17. It is important to note that, although the association between the variables was already calculated through linear regressions before (Tables 15, 16 and 17), the significance level of α was not adjusted due to (i) the datasets are not equal (as mentioned above), and (ii) the purpose of Table 18 is merely illustrate the calculated Pearson correlation coefficients for the complete dataset.

Higher Frequencies components of HRV showed an inverse correlation with the expression of surface MPO (measured either as percentage or mean fluorescence intensity) and an

inverse, non-significant correlation, with the number of circulating number of MPs (Annexin+ MPs).

In the time domain, SDNN showed an inverse correlation with Annexin+ MPs (-0.38, p-value < 0.05) and the expression of myeloperoxidase by granulocytes (-0.35, p-value < 0.05), when measured as a percentage of granulocytes expressing it on the membrane surface. It is interesting to note that RMSSD demonstrated a higher correlation with the SDNN and the Higher Frequencies than with the Lower Frequencies.

Correlation was also negative for FMD Index and Annexin+ MPs and MPO measured by both, percentage of granulocytes expressing it in the membrane surface or as mean fluorescence intensity, although not statistically significant for the second (p-values > 0.05).

There were strong, statistically significant correlations between MPO MFI and neutrophils (-0.55, p-values < 0.05), and significant positive correlation between the percentage of granulocytes expressing MPO in the membrane surface (MPO%) and neutrophils (0.70, p-values < 0.05).

The inverse association between HRV in the frequency domain and the total number of circulating MPs, observed in Tables 15 and 16, is also clearly present in the correlation analysis (p-value < 0.05).

Lower Frequencies presented a non-significant (p-value = 0.06) negative correlation with total number of MPs (Table 16), while the Lower Frequencies as a proportion of total variability (LF Ratio) does not seem to correlate with other variables

There are strong positive correlations between CD41+ MPs, platelets and neutrophils counting (p-values < 0.001), and a significant negative correlation between CD41+ MP and MPO (p-value < 0.05). Circulating platelets showed a strong significant negative correlation with MPO measured as mean fluorescence intensity (MFI) (-0.65, p-value < 0.001).

Table 18. *Pearson correlation analysis*

	CD16 (%)	CD66b MFI	FMD Index	HF abs	HF Ratio	LF abs	LF Ratio	MP CD31 +	MP CD41 +	MP CD66b +	MPO (%)	MPO (MFI)	Neutrophils	Platelets	RMSSD	SDNN
Anexx +	0.116 p-value: 0.4958	0.473 p-value: 0.0031**	-0.368 p-value: 0.0251*	-0.289 p-value: 0.0826	-0.127 p-value: 0.4523	-0.306 p-value: 0.0659	-0.114 p-value: 0.5025	-0.121 p-value: 0.474	-0.2 p-value: 0.2353	-0.171 p-value: 0.3129	0.454 p-value: 0.0048**	0.709 p-value: 0***	-0.457 p-value: 0.0045**	-0.495 p-value: 0.0018**	-0.291 p-value: 0.0803	-0.383 p-value: 0.0193*
CD16 (%)		-0.119 p-value: 0.484	-0.003 p-value: 0.9878	-0.082 p-value: 0.6313	0.073 p-value: 0.6683	-0.279 p-value: 0.0944	-0.032 p-value: 0.8497	0.293 p-value: 0.0783	-0.071 p-value: 0.6746	-0.098 p-value: 0.5653	0.23 p-value: 0.1705	-0.08 p-value: 0.6374	0.142 p-value: 0.4032	0.109 p-value: 0.5225	-0.207 p-value: 0.2187	-0.205 p-value: 0.2229
CD66b MFI			-0.073 p-value: 0.6689	-0.198 p-value: 0.2404	-0.12 p-value: 0.4802	-0.206 p-value: 0.2212	-0.351 p-value: 0.0331*	0.229 p-value: 0.172	-0.373 p-value: 0.023*	-0.068 p-value: 0.6872	-0.074 p-value: 0.6644	0.373 p-value: 0.023*	-0.663 p-value: 0***	-0.625 p-value: 0***	-0.057 p-value: 0.7373	-0.175 p-value: 0.2997
FMD Index				-0.033 p-value: 0.8448	-0.086 p-value: 0.6147	0.209 p-value: 0.2147	0.134 p-value: 0.4302	0.095 p-value: 0.5745	0.09 p-value: 0.5969	0.191 p-value: 0.2564	-0.185 p-value: 0.2722	-0.253 p-value: 0.1313	0.27 p-value: 0.1055	0.238 p-value: 0.1554	0.039 p-value: 0.8184	0.138 p-value: 0.4147
HF abs					0.622 p-value: 0***	0.689 p-value: 0***	0.07 p-value: 0.6795	0.001 p-value: 0.9936	0.214 p-value: 0.2042	0.173 p-value: 0.3046	-0.397 p-value: 0.015*	-0.318 p-value: 0.0548	0.158 p-value: 0.3515	0.074 p-value: 0.6616	0.833 p-value: 0***	0.881 p-value: 0***
HF Ratio						0.262 p-value: 0.1173	0.324 p-value: 0.0502	0.158 p-value: 0.3492	0.086 p-value: 0.6142	0.125 p-value: 0.461	-0.289 p-value: 0.0826	-0.249 p-value: 0.1368	0.01 p-value: 0.9517	0.147 p-value: 0.3849	0.564 p-value: 0.0003***	0.262 p-value: 0.1178
LF abs							0.428 p-value: 0.0082**	-0.144 p-value: 0.3954	0.272 p-value: 0.1028	0.277 p-value: 0.0963	-0.256 p-value: 0.1257	-0.14 p-value: 0.4072	0.201 p-value: 0.2337	0.13 p-value: 0.4419	0.563 p-value: 0.0003***	0.794 p-value: 0***
LF Ratio								-0.144 p-value: 0.3967	0.113 p-value: 0.5054	-0.018 p-value: 0.9165	0.19 p-value: 0.2607	0.124 p-value: 0.466	0.09 p-value: 0.5956	0.228 p-value: 0.1756	-0.04 p-value: 0.8153	-0.01 p-value: 0.9551
MP CD31 +									-0.111 p-value: 0.5121	0.129 p-value: 0.4459	-0.157 p-value: 0.3521	-0.244 p-value: 0.1463	0.096 p-value: 0.5724	0.068 p-value: 0.6898	0.004 p-value: 0.9832	-0.083 p-value: 0.6241
MP CD41 +										0.226 p-value: 0.1778	-0.204 p-value: 0.2258	-0.409 p-value: 0.0119*	0.542 p-value: 0.0005***	0.585 p-value: 0.0001***	0.152 p-value: 0.3678	0.22 p-value: 0.1917
MP CD66b +											-0.32 p-value: 0.0537	-0.25 p-value: 0.1363	0.177 p-value: 0.2946	0.199 p-value: 0.2368	0.258 p-value: 0.1225	0.244 p-value: 0.1448
MPO (%)												0.709 p-value: 0***	-0.017 p-value: 0.9201	-0.228 p-value: 0.1744	-0.38 p-value: 0.0203*	-0.356 p-value: 0.0305*
MPO (MFI)													-0.55 p-value: 0.0004***	-0.652 p-value: 0***	-0.284 p-value: 0.0886	-0.28 p-value: 0.0938
Neutrophils Ratio														0.857 p-value: 0***	0.03 p-value: 0.8593	0.163 p-value: 0.3352
Platelets															-0.052 p-value: 0.7579	0.001 p-value: 0.9942
RMSSD																0.789 p-value: 0***

Correlation coefficients and p-values are shown for the data set for which all infomartion was available. "*" p-value < 0.5, "**" 0.01 > p-valeu > 0.001, "***" p-value < 0.001

Modeling

As defined in the Materials and Methods session, mathematical modeling was made using RBF-NN. First, the whole dataset, disregarding the experimental profile utilized (N = 47), was used for the RBF-NN calibration. The data set was organized so that the pre and post dive variation of the CD16(%), CD66b (MFI), MPO(%), MPO (MFI), Anexxin +, MP CD66b +, MP CD31+ and MP CD41+ were used to explain the variation of the HRV indicator SDNN, or simply SDNN Ratio, as previously defined.

As previously described, Gaussian functions were chosen for activation and the model was based on the neural network that produced the best accuracy for the training set in 10.000 trials, in a stochastic process of centroids determination. As detailed in the Material and Methods section, the number of clusters used to create the RBF-NN was based on a decay curve approximation of the sum of the within distances. The number of clusters was chosen to account for approximately 60% of the sum of distances (Figure 19).

This model, created to estimate the variation of the SDNN Ratio (Figure 15) as a function of the variation of the CD16(%), CD66b (MFI), MPO(%), MPO (MFI), Anexxin +, MP CD66b +, MP CD31+ and MP CD41+, produced a Training Accuracy of 0.16 (expressed as RMSE), demonstrating that it is possible to use the variation of the observed variables to explain the variation of HRV, as measured by SDNN .

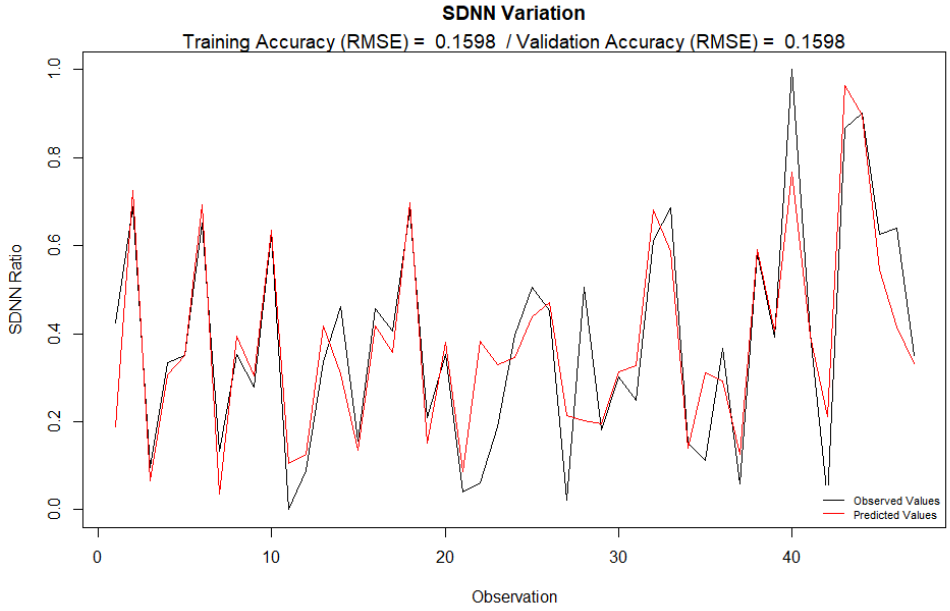

Figure 15. Observed and calculated SDNN Ratio based on the variation of CD16(%), CD66b (MFI), MPO(%), MPO (MFI), Anexxin +, MP CD66b +, MP CD31+ and MP CD41+ . It is important to note that Training Accuracy and Validation Accuracy are the same due to the fact that the model is being applied on the training set (in-sample validation). This test was done to evaluate how effective the algorithm is in reproducing the data used for calibration.

In order to test the robustness of the modeling process, further tests were performed. Firstly, a second model was created, where the calibration of the RBF-NN was done using only a portion of the data (N = 37), chosen in a stochastic process. As in the first model, Gaussian functions were chosen for activation and the model was based on the neural network that produced the best accuracy for the training set in 100 trials, in a stochastic process of centroids determination. The model created was then applied to the remaining 10 observations in an out-of-sample validation process, producing a Training Accuracy of 0.1361 and a Validation Accuracy of 0.1237 (Figure 16). Interestingly, the training accuracy was slightly higher than the first model, even with the use of a smaller dataset for training in comparison with the in-sample applied model display in Figure 15. The similarity of the Training and Validation Accuracies reinforces the predictive capability of the model, while providing support that the model was not overfitted.

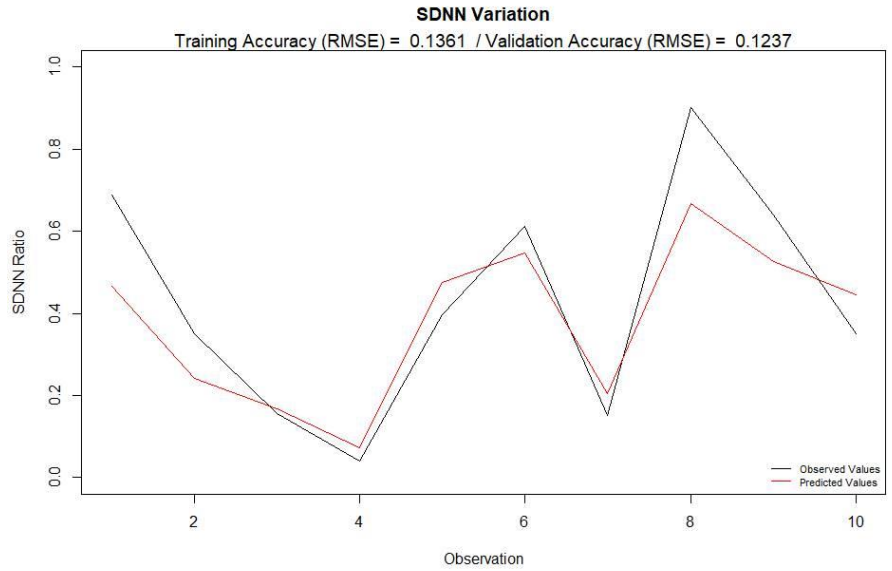

Figure 16. Observed and predicted SDNN Ratio based on the variation of CD16(%), CD66b (MFI), MPO(%), MPO (MFI), Anexxin +, MP CD66b +, MP CD31+ and MP CD41+ . Application of the second model on an out-of-sample data set.

Secondly, through the utilization of a stochastic resampling technique, 2.000 new datasets were created divided in: (i) 1.000 containing part of the data (N = 37) (training datasets) and (ii) 1.000 containing the remaining part of the data (N = 10), that were not used in the respective training dataset creation (validation datasets). Again, Gaussian functions were used for activation and each model was based on the neural network that produced the best accuracy for each training set in 100 trials, in a stochastic process of centroids determination, and subsequently applied to the respective validation dataset. This process was used to estimate the distribution of the error of the modeling process when applied to different training and validation datasets (Figure 17).

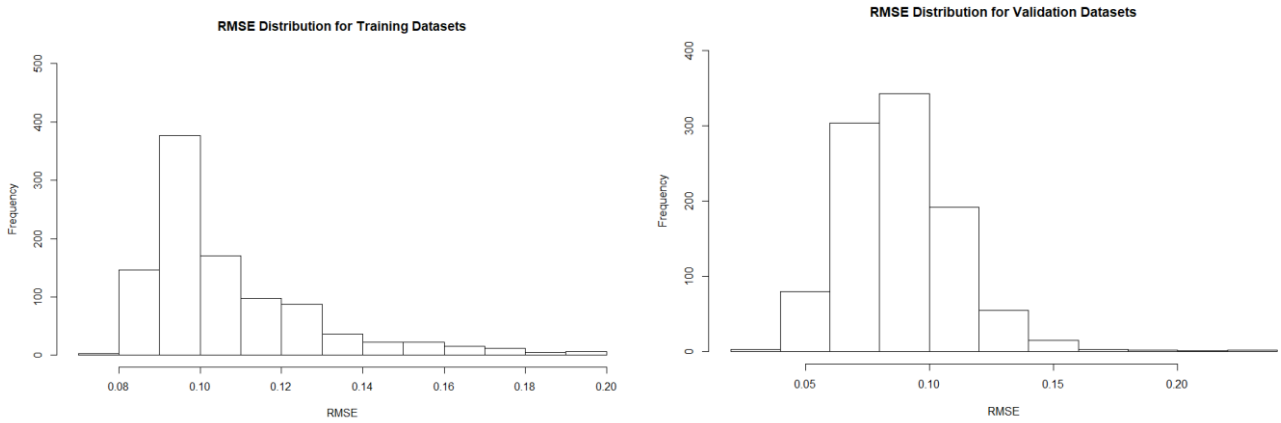

Figure 17. Training and validation error distribution produced by the 1.000 models created based on the resampled data.

The data above can be summarized by the mean error in the training and validation process, illustrated in Figure 18. Interestingly, similarly to the model demonstrated above, the mean error observed during the training of the RBF-NN is slightly higher than the mean error observed in the application of the model to the validation datasets, reinforcing prediction capabilities of the model and the relationship between the observed variables.

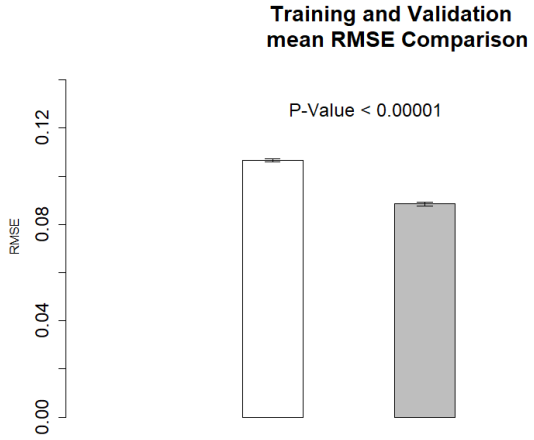

Figure 18. Mean error observed during the training and validation processes of the models created based on resampled datasets. Note that the mean training error (0.1066) is slightly higher than the mean validation error (0.0885).

It is important to note that all the data was normalized, according to the normalization method described in the Materials and Method section. Both, the normalized and the original data sets, are herein attached as Appendixes IV and V, respectively.

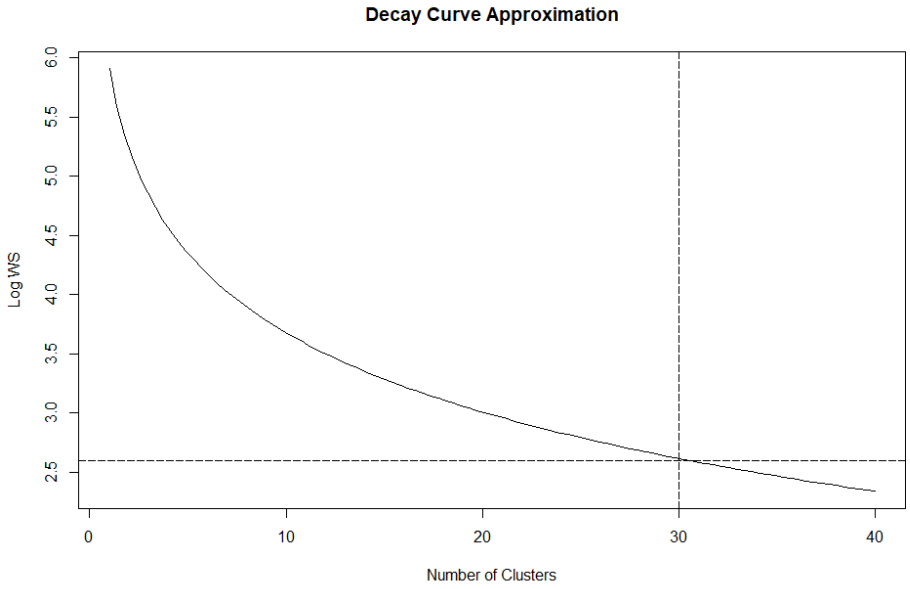

Figure 19. Estimated decay curve of the within sum of distances as function of the number of clusters. Note that the WS variation was not calculated for more than 40 clusters.

Case Study: Y – 40 Swimming pool shallow decompression profile

As previously mentioned, the results obtained during the experiment held at the Y – 40 swimming pool, in which a shallower decompression profile was applied, were not included in this study due to the fact that such decompression profile caused many theoretical compartments of the decompression model to greatly exceed the supersaturation limits applied to all other experiments, in a manner that the results obtained are not comparable to the others upon which this study was prepared. The results obtained in this profile, however, brought interesting information that may add to the overall understanding of the matter, and will, therefore, be reported here as a case study.

Table 19 below displays the pre and post HRV indicators per volunteer, as well as the group means.

Table 19. *Heart Rate Variability Indicators*

	SDNN (ms)		LF (ms^2)		HF (ms^2)		LF / HF	
	Pre	Post	Pre	Post	Pre	Post	Pre	Post
Volunteer 1	55,62	56,02	410,10	878,57	52,75	97,56	8,82	9,03
Volunteer 2	38,60	33,28	382,26	304,62	32,08	13,02	12,50	24,67
Volunteer 3	32,70	27,83	152,90	146,25	8,67	10,38	18,75	16,11
Volunteer 4	48,72	36,25	512,08	329,45	203,93	23,99	2,96	11,85
Mean	43,91	38,35	364,34	414,72	74,36	36,24	10,76	15,42

An overall reduction in variability, given by SDNN, with a decrease in the Higher Frequencies accompanied by an increase in the LF/HF ratio, is observed in this group.

Flow cytometry was not performed in this experiment, therefore immune system activation markers and MPs analysis are not available to be correlated with the changes observed in the HRV indicators. However, the changes observed in hematocrit and hemoglobin are compatible with the results obtained in other experiments (Table 20) and, although they are apparently greater in magnitude, the experimental sample is too small for any hypothesis test to be performed.

Table 20. *Blood Assay*

	Hematocrit		Hemoglobin	
	Pre	Post	Pre	Post
Volunteer 1	41	36	12	11
Volunteer 2	45	35	15	12
Volunteer 3	41	42	14	14
Volunteer 4	43	45	15	15
Mean	42.5	39.5	14.0	13.1

Note: data collected by DAN Europe

Discussion

It is well documented that exposure to hyperbaric environments and subsequent decompression has many physiological implications, ranging from reduction in endothelial function to activation of the immune system. As previously mentioned, post decompression formation of bubbles is a common finding in subjects exposed to hyperbaric environments. Although it is widely accepted that decompression sickness is caused by bubbles formed during decompression, venous gas emboli are a poor surrogate for decompression sickness [13], and the causal relationship between them and other decompression-related physiological alterations, if any, is yet to be understood [14].

The endothelial dysfunction hypothesis [15], which postulates that microparticles associated with endothelial damage may act as nucleation sites for bubble formation, is based on the observation of increased numbers of MPs after hyperbaric exposures. These MPs are shed by different cells in an organized and regulated manner, are involved in cell signaling and communication, and serve as relevant markers of inflammatory diseases [16]. It could be speculated that MPs act as nucleation points, causing observed bubbles to be, among other things, a consequence of the existence of such MPs in a media supersaturated by inert gases. The correlation between bubbles and MPs counts has been studied [11], but no conclusive results have been found (in fact, the data published in the referenced report indicates a surprising negative correlation between bubbles and MPs).

Previous studies have shown that exposure to hyperbaric ambient and subsequent decompression is associated with HRV changes [36 37 57]. Immersion and inspiration of higher partial pressures of oxygen is associated to HRV changes as well [58], even before the start of the reduction in the ambient pressure, during the decompression phase of the exposure, or the ascent in the case of SCUBA diving.

Our previous study [36] reported an apparently disproportioned increase in the Lower Frequencies of the HRV, causing a shift of the total power towards the left of the

spectrogram. Whether these changes were related to other physiological changes known to be associated with decompression was speculated. The results obtained from a control group used in our previous research, that followed the same protocol applied during the simulated dive, while not exposed to an ambient pressure increase demonstrated a significant overall increase in the lower and higher frequencies of the Heart Rate Variability in the frequency domain, as well as the total variance in the time domain, given by SDNN.

In the present study, a correlation between changes in both, the sympathetic and the parasympathetic tones of the Autonomous Nervous System observed after decompression, with other indicators of physiological stress known to be associated with decompression and, ultimately, with decompression sickness was made. In this context, physiological stress might be defined as the inflammation and activation of the immune system processes that are, apparently, tied to the oxidative stress caused by the compression-decompression process [11] [59].

Up to this date, more than one hundred years after the study published by Haldane et al., the nature of decompression sickness, i.e., whether it should be classified as an inflammatory disease, or as a consequence of mechanical damage caused by bubbles, or even as a combination of both, is far from the end. Although the role of the inflammation process associated with decompression has gained support in the past decade [15] [14], the perception that decompression sickness is mainly due to the appearance and growth of bubbles is still very much accepted. A series of three articles recently published assume that the symptoms of decompression sickness are due to tissue perfusion alterations that, ultimately, causes the pressure of inert gas to raise enough to produce bubbles in a specific location [60] [61] [62]. Concomitantly, the possibility of MPs acting as nucleation points, which would link the observation of MPs to bubbles, is still under investigation and cannot be ruled out [63]. An ongoing research conducted by the Laboratory of Energetics and Theoretical Physiology of the University of Sao Paulo (results not yet published), has obtained interest results in modeling the appearance of bubbles and estimated inflammation processes, through the interaction of expected bubble formation and pro-inflammatory factors. An example of the results obtained up to this point are illustrated in Appendix III.

In regard to HRV and decompression, studies from the same research group in swine model reported contradictory results. One study reported a reduction in the two branches of the Autonomic Nervous System (ANS) activity, when symptoms of decompression sickness are present [64], while the second reported an elevated parasympathetic activity, with increased power associated with the Higher Frequencies, during the development of cardio vascular decompression sickness (characterized by breathing difficulties, hemoptysis, dyspnea and considered a serious manifestation of decompression sickness), as well as a decrease in the sympathetic branch activity when compared to the baseline pre dive values [65]. Interestingly, the second study reported a significant increase in SDNN and in the Higher Frequencies of spectrogram immediately after surfacing and even before any symptom of decompression sickness could be identified. They also reported an increase in the parasympathetic activity, calculated using the PDM method. Moreover, it does demonstrate that as the time after the end of decompression increases, a decrease in the frequency domain indicators of HRV happens in the group diagnosed with decompression sickness in comparison with the control group, affecting especially the sympathetic tone, with impact in the overall variability measured by SDNN. It is worth to note that the experimental protocols adopted by the two studies, in terms of exposure, were not comparable and that the animals used in the first study, that reported reduction in the activity of the Autonomic Nervous System, received diazepam. Diazepam is known to be associated with an overall reduction of Heart Rate Variability in humans and it appears to be a fair assumption that it could cause a similar reduction in swine [66], potentially affecting the results reported in the study.

Frequency domain components of HRV were reported to be inversely correlated with inflammation markers by at least one large scale study [44]. Additionally, a review of thirteen studies about HRV and inflammation, in the same line, reported an inverse relationship between inflammatory markers and the time and frequency domain indicators of HRV in cardiovascular disease [67].

Vagal activity has also been positively correlated with endothelial function. A study with 46 male, healthy individuals, found significant positive correlations between endothelial

function, assessed by measuring brachial artery flow mediated dilation, and three HRV indicators: SDNN and RMSSD in the time domain and the Higher Frequencies in the frequency domain [68]. This association is specifically interesting for the present study, since SCUBA diving and decompression, in particular, is known to be associated with endothelial dysfunction.

Endothelium is a highly specialized tissued that regulates vascular tone, leukocyte adehesion, platelet aggregation, and plays a protective role triggered by stimuli, such as the shear stress caused by blood flow against its cellls, which results in a basal production of oxide nitric (NO), a neurotransmitter responsible for mainting vasodilation through the relaxation of the smooth muscle. NO is paracrine and autocrine signaling molecule, generated by L-arginine by the action of endothelial NO synthase (eNOS) in the vascular wall, which mainly targets guanyllate cyclase, leading to cGMP-mediated the relaxition of the smooth muscles and, therefore, vasodilation. Nitric oxide exerts a potent antiatherogenic effect, preventing platelet adhsesion and aggreation [69]. Endothelial dysfunction might be defined as the loss of endothelium-dependent relaxation, caused, among other things, by the reduced bioavalability of NO.

The data collected in this study corroborates previous observations that endothelial function is negatively affected by the exposure to hyperbaric ambients and subsquent decompression. Figure 11 demonstrates that most of the participants of this research lost endothelial responsiveness after decompression. More interestingly, it becomes clear in Figure 10 that different decompression profiles caused different outcomes, in terms of mean wave amplitude, when mesaured by pre and post occlusion PWA, where the Deeper Decompression Profile was related to an increased vasocontriction. Altough it is interesting to note the significant PWA differences, it is important to one more time to enphasize that PWA is not the best method to measure vasoconstriction or vasodilation in different moments, due to the fact that the readings obtained might not be comparable.

In the present protocol, MPO levels were observed as a marker of neutrophils activation. MPO is an enzyme most abundantly expressed in neutrophils and, to a lesser extent, in

monocytes. This enzyme has long been viewed as functioning primarily as a bactericidal agent, generating reactive oxygen species (ROS) that contribute to the destruction and killing of the engulfed pathogens [70] . It has been demonstrated that MPO is involved in cellular homeostasis and plays an important role in the initiation and progression of acute and chronic inflammatory diseases [71]. MPO reduces H_2O_2 to oxidize chloride, a reaction which yields HOCl. HOCl is known for its ability to modify diverse molecules via chlorination. In the vasculature, MPO-generated HOCl has been shown to affect eNOS activity and to decrease NO bioavailability, thereby negatively affecting endothelial function. In fact, it was demonstrated that MPO is involved in depleting vascular NO bioavailability: MPO knockout mice, exposed to an acute inflammatory stimulus displayed improved vascular function and increased vascular NO bioavailability as compared to wild-type mice, suggesting that subendothelial MPO is a significant contributor to impaired NO bioavailability in vivo [71]. MPO was demonstrated to be associated with neutrophils activation, through the activation of intracellular signaling cascades, which increase ROS production. Recently, MPO has emerged from a marker of neutrophil activation to an enzyme deeply involved in the pathogenesis of inflammatory vascullar disceases, that are, in many aspects, similar to ones observed in decompression sickness [71].

Based on the above, it is likely that the loss of endothelial responsiveness and the increased levels of MPO are associated, in line with the negative correlation observed in Table18 (even though not statistically significant). A previous study that evaluated, among other things, MPO levels in divers suffering from decompression sickness and in a control group, reported a significant increase in both percentage of MPO expression (MPO+ %) and mean fluorescence intensity (MPO MFI) in divers diagnosed with decompression sickness [10]. Blood samples were taken when divers presented themselves for treatment, after the onset of decompression sickness simpthoms, therefore a few hours after the end of decompression (average interval was not reported). There was a significant increase in MPO MFI in the control group as well, for which blood samples were obtained two hours after the dive. In their report it is not clear whether or not dead cells were excluded during the Flow Cytometry execution. In the present protocol, an exlusion of dead cells was made, due to the fact that after cell death, the membrane will lose its integrity, allowing antibodies to

mark inespecifc intracellular sites, or, in the case of MPO, intracellular molecules. Since MPO account for 5% of the dry weight of neutrophils, marking intracellular molecules due to membrane corruption will affect the observed results [72].

Increased post dive values of MPO are probably associated with the increased number of circulating neutrophils observed and their activation. This increased number of neutrophils might be a response to an inflammatory process, which is also expected to increase the synthesis of interleukin 6 (IL-6), tumor necrosis factor alpha (TNF)-α and C-reactive protein (CRP) [73]. CRP is known to reduce eNOS acticity, therefore reducing NO availability and consequently endothelium-dependent vasodilation [74]. The present study, however, did not monitor IL-6, TNF-α and CRP levels, therefore such association, although logic, can only be especulated for the time being. Duplicates of all samples obtained in this study were frozen for an eventual future reevaluation.

A reduction in the number of circulating platelets was also observed in both experimental profiles, being statiscally significant in the Deeper Decompression Profile. Platelets have long been described as effectors of hemostasis, being essential for vascular integrity. More recently the understanding that they are key effectors in inflammantion, immune responses and signalying functions, having the potential to orchestrate complex immune and inflammatory events is becoming clearer [75] [76]. Three different studies designed by the same research team investigated platelet counts and its association with decompression sickness in mice models and with buble formation in humans [77] [78] [79]. Their results indicate that higher bubbles counts in humans correlate with more pronounced fall in platelets, even in the absence of decompression sickness, after decompression, while in mices suffering from decompression sickness after provocative decompression, a regression model could associate the platelet reduction with the severity of the sympthoms. In both cases, they especulated that such reduction was due to platelet activation and aggregation. Another study, published by the US Navy in 1970´s, reported a markely decrease in platelets numbers followed by an increase in megathrombocytes (large young forms of platelets that become progressively smaller with age) in humans after exposures to 6.7ATA [80]. Increased megathrombocytes numbers were, in this case, used to detect thrombocytolytic states, since

in a condition of high platelet utilization, a rise in the percentage of megathrombocytes may occur. The same study reported that the observed increased percentage of megathrombocytes, could be associated with either increased production or decreased destruction of smaller platelets, therefore reflecting high platelet turnover.

The reduced post dive numbers of platelets herein reported is compatible with their activation and recruitement to inflammation sites. The inverse correlation between (-0.65, p-value < 0.001) platelets and the expression of MPO observed in this study offers strong support to this argument [81] [82], although other reasons for a reduction platelets numbers cannot be excluded (such as, for instance, platelet destruction).

Activated platelets release microparticles (CD41+ MPs) that might work as a mechanism for intercellular (endogenous) signaling by inducing immune responses in distant sites. There are in-vitro evidences that CD41+ MPs contribute to leukocyte – leukocyte interactions, involving the binding of P-selectin / P-selectin glycoprotein ligand-1 (PSLG-1), increasing accumulation of leukocytes at site of injury and on activated endothelium. Additionally, platelet shedding of MPs positively correlates with signs of increased vascular permeability [83]. The results obtained in this study points to an increase in the number of circulating CD41+ MPs after decompression, with a notable significant increase in the Deeper Decompression Profile, which is compatible with the reduction in the numbers of circulating platelets, due to the previously mentioned assumption that it would be due to their activation and recruitment to inflammation sites (Tables 13 and 14).

The contributions of MPs to the inflammatory process is becoming progressively better understood. The release of platelet, endothelial and leukocyte MPs is increased during inflammatory conditions [84]. Activation by inflammatory cytokines, ROS and stimulus TNF-α are known to result in the release of endothelial-derived MPs (CD31+ MPs). Oxidative stress is known to cause the release of CD31+ MPs, which ultimately attract leukocytes to the inflammatory site by adhesion molecules, such as vascular cell adhesion molecule-1 (VCAM-1), which is intimately linked to endothelial dysfunction [85].

Our results demonstrate an increase in endothelial derived MPs (CD31+ MPs) post dive, again with a steeper increase in the Deeper Decompression Profile (Tables 13 and 14 and figure 11).

The results obtained in the present study demonstrated that MPs subtypes have little and not statistically significant correlation among each other, which contradicts another study previously published [10]. The reason for contradiction would require further investigation. In the same line, the post dive magnitude of all MPs subtypes mean increase reported by the same study is greater than the mean increase observed in the present study.

Interestingly, leukocyte-derived MPs (CD66b+ MPs) appears to carry an endogenous anti-inflammatory cytokine that stimulates the production of transforming growth factor β1 (TGF β1), acting to control inflammation at its early stages [16]. Other studies report the anti-inflammatory role of CD66b+ MPs by not only enhancing the release of TGF β1, but also decreasing macrophage activation. During our experiments, we observed a negative correlation between CD66b+ MPs and MPO (-0.32, p-value = 0.05). We also observed a maintenance of the levels of CD66b+ MPs in the Deeper Decompression Profile, and a significant increase in their levels in the Shallower Decompression Profile. It is worth to note that, although a causal relationship cannot be established, other inflammatory markers alterations and the different levels of CD66b+ MPs (i.e. MPO) in the different experimental protocols offers support to infer an anti-inflammatory role of the CD66b+ MPs. Due to the lack of specific controls, this study, can only speculate that the higher levels of CD66b+ MPs observed are associated with the post dive lower levels of MPO detected in the Shallower Decompression Profile.

In a contrary direction, a study designed to evaluate the association of MPs and decompression sickness reported a post dive 30-fold increase in CD66b+ MPs, even in the absence of decompression sickness, causing the anti-inflammatory role this MP subtype speculated above to be void and demonstrating a high positive correlation between MPO and leukocyte-derived MPs [10].

Both profiles caused a reduction in erythrocytes, hematocrit and hemoglobin, with, again, a greater decrease in the results obtained from the Deeper Decompression Profile (Tables 9 and 10), although the post dive results from both profiles do not present significant difference among each other (p-value > 0.05, Figure 13). This result is also in line with other results obtained by research teams working in collaboration with the Laboratory of Energetics and Theoretical Physiology of the University of Sao Paulo and with a study designed to evaluate changes in hematological parameters after SCUBA diving[86]. It could be speculated that one possible explanation for this reduction is eryptosis, a form of programmed cell death undergone by erythrocytes, known to be triggered by oxidative stress, in a mechanism where caspases expressed by erythrocytes are activated, resulting in the erythrocytes being recognized and engulfed by circulating macrophages. Since the erythrocyte membranes are very vulnerable to oxidative damage and erythrocytes are unable to repair damaged components as proteins by re-synthesis, they are very sensitive to oxidative stress [86].

NO also plays an important role in this mechanism, since it is released from deoxygenated hemoglobin in erythrocytes and inhibits erythrocytes death, due to its role in vasodilation in tissues which are hypoxic, by activating G protein kinase, known to be important to erythrocyte survival. The increased MPO values and reduction in the FMD index observed in this study are compatible with an increased production of ROS, reduction in the bioavailability of NO and, therefore, increased levels of erythrocytes death due to oxidative stress, providing support for the reduction in the red cells and hemoglobin observed after the experimental profiles. It is important to note, however, that the erythrocytes death, observed in the present study and in others before, was not observed in by other studies when inert gases were not present in the breathing mix, and it has been reported that hyperbaric oxygen (HBO) exposure is not associated with blood count changes [87]. The fact that hyperbaric oxygen exposures are not related to erythrocytes death, even while causing massive oxidative stress, challenges the understanding that oxidative stress alone would trigger erythrocytes death (or eryptosis, as mentioned above), otherwise a decrease in erythrocytes numbers would be expected after HBO exposure.

A possible explanation for this paradox could be the elevated levels of NO production associated with HBO, which, by the mechanism described above, could inhibit erythrocytes death. In an animal study designed to assess the mechanism behind oxygen toxicity to the Central Nervous System, it was observed that an exposure to pure oxygen at a pressure of 3 ATM (303 kPa) would cause a ~4.5-fold increase in the production of NO [88]. The study hypothesized that increased availability of oxygen due to HBO would increase NOS activity, therefore increasing NO levels.

Interestingly, it has been shown that hyperbaric exposures where nitrogen or helium are present in the breathing mix are associated with post decompression endothelial dysfunction, while the exposures made with pure oxygen are not [22] , fact that could be linked to the NOS activity and consequent NO production described above. However, further research is necessary in order to clarify this apparent contradiction.

The primary objective of this study was to evaluate the feasibility of using HRV as an indicator of the decompression related physiological stress. The results obtained demonstrated that HRV indicators, in special SDNN, as a broader indicator of variability in the time domain, and the Higher Frequencies in the frequency domain, are significantly negatively correlated with different markers of inflammation and immune system activation provoked by the exposure to hyperbaric environments and subsequent decompression. Increased expression of myeloperoxidase on neutrophils surface, as well as increased number of circulating Annexin+ MPs are associated with reduced variability, either measured by SDNN, or by power associated with the sum of all frequencies, approximated by $SDNN^2$. Higher Frequencies of the spectrogram are known to have higher correlation with the total variance and, as expected, demonstrated inverse correlations with MPO and the number of circulating MPs as well. On the other hand, the Lower Frequencies, apparently, are less sensible to the variation of the observed markers.
Another possible support to the utilization of HRV as an indicator of the decompression related physiological stress comes from the relationship between endothelial function, given by the FMD Index, the Higher Frequencies, in the frequency domain, and SDNN and RMSSD, in the time domain (Table 17). In line with a previous study made with healthy

subjects not exposed to hyperbaric environments [68], the results obtained in the present study demonstrated a significant positive correlation between Higher Frequencies, SDNN and RMSSD with the FMD Index. These results are consistent with the inverse correlation between endothelial function, HRV and increased levels of MPO also observed in the present study.

We observed in our previous research that the exposure to high fractions of oxygen, even in the absence of changes in the ambient pressure, is associated with increased Heart Rate Variability measured in both, the time and frequency domains [36]. It is plausible that general post dive increase in the HRV observed in this (and in other previously published studies) is related to the hyperoxia almost inherently linked to the exposure to hyperbaric environments. A possible explanation for the disproportional elevation in the Lower Frequencies might be that endothelial dysfunction causes changes in the baroreceptor activity. Lower Frequencies are intimately linked to baroreflex function, as previous studies demonstrated that carotid sinus stimulation increases Lower Frequencies power in individuals with normal baroreflex function, but not in those with impaired baroreflex sensitivity [89] [40]. Additionally, Lower Frequencies have been negatively correlated with endothelial function [46]. The ANS and the endothelium work together to maintain vascular tone. There is a tonic balance between the release of vasodilating factors from the endothelium and vasoconstricting factors triggered by the sympathetic branch of the ANS. The balance between these opposing forces acts on the vascular smooth muscle cells to maintain the appropriate vessel tone [90]. The disturbance of this tonic balance, due to the reduced NO availability, may be the reason why sympathetic activity is associated with loss of endothelial function in some circumstances.

As mentioned above, Higher Frequencies have greater sensitivity to increased levels of inflammation markers, as observed in many volunteers, accentuating even more the post dive disproportional increase (due to Higher Frequencies decrease) of the Lower Frequencies as a ratio of total variability. Frequency Variation Ratio (FPR), as defined in equation 26, was used in an attempt to capture the pre and post simulated dive relative

contributions of both, Lower Frequencies and Higher Frequencies for the total variability. The increased post dive relative participation of the Lower Frequencies showed an inverse correlation with the FMD Index, even though not statistically significant (Table 17). As previously mentioned, the post dive PWA was lower in both decompression profiles, although statistically significant only for the Deeper Decompression Profile (figure 10), which might be due to the combination of increased sympathetic activity and lower availability of the endothelium-derived relaxing factor NO.

Based on the above, reductions in HRV, in special overall variance, given by SDNN and Higher Frequencies, due to its high correlation with SDNN, might be associated with increased levels of decompression-related physiological stress and, in this case, HRV could to be a good predictor of decompression-related physiological stress. The accuracy of the model created to predict the pre and post dive rate of variation of the SDNN based on variation of inflammatory markers and number of circulating MPs (Figure 15 and 16) provides further evidence of the correlation between physiological stress markers and HRV, corroborating the understanding it might be a good measurement of decompression-related physiological stress.

However, the above-reported relationship between SDNN, Higher Frequencies, in the frequency domain, and the variables used in this study as markers of physiological stress might not hold true in cases where there are evident symptoms of decompression sickness. In the one single case of decompression sickness diagnosed during the experimental protocol, an increase in the SDNN and in the Higher Frequencies of the spectrogram was observed, notwithstanding the significant increase in all markers of inflammation and immune system activation, in special the MPO values (post experiment MPO expression was 1.4x the pre experiment value).

One possible explanation for this different HRV pattern might be the symptoms associated with decompression sickness reported by the volunteer, still during the ECG recording that was later used for HRV calculation. It could be expected that, whenever there are manifestations of symptoms related to decompression sickness, not only the pain, but the anxiety experimented by the individual at this point, would directly affect diverse

physiological variables, among them ventilatory rate and blood pressure, thus indirectly affecting HRV as well. Not to mention potential decompression sickness related neurological impairment that might cause other alterations on its own. Interestingly, the results observed in this case, where decompression sickness symptoms were present, are comparable with the ones published by the study that submitted animals to provocative decompression [65] and reported increased SDNN, Higher Frequencies and parasympathetic activity in animals suffering from cardiovascular decompression sickness. The same study reported a progressive loss of HRV in the same animal group as the time after decompression passed. In the present study, the EGC recordings for HRV calculation were made in one single interval (as described in the Material and Methods section), therefore it is not possible to speculate how HRV indicator behaved more than one hour after the end of the decompression.

It is well understood that different decompression profiles generate different tissue supersaturation upon surfacing. It is also known that the composition of the breathing gases (i.e. the fraction of oxygen and the presence of helium), causes different physiological responses. At least one previous study has demonstrated that the addition of helium in the composition of the breathing gas is associated to a lower reduction in the post dive platelet count [21]. It might be possible to speculate the existence of a dose-dependent kind of response, where, for a given subject, lower tissue supersaturation would lead to little or no physiological alterations, while higher tissue supersaturations would lead to progressively greater physiological responses, in a process that would eventually culminate with the development of decompression sickness.

In this study, it becomes clear that two experimental profiles, with the same total exposure, in terms of time, ambient pressure and breathing gases, but with decompression stops time and depth distributed differently, produced different physiological results. In figure 20, below, the inner compartment pressure difference in relation to the ambient pressure over time is illustrated by different colors, according to the legend.

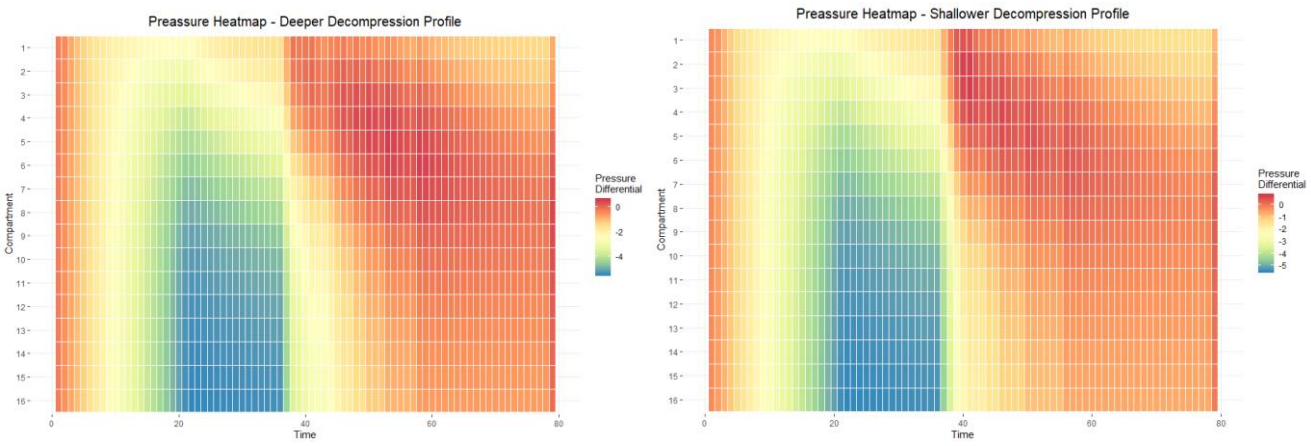

Figure 20. In the y-axis, compartment number 1 represents the fastest hypothetical tissue, while compartment number 16 represents the slowest one. The x-axis represents time from the beginning of the exposure until the end of the decompression process. The Shallower Decompression Profile caused a greater supersaturation in the faster compartments at the beginning of the ascent, marked by the darker red at the top of the chart, not observed in the Deeper Decompression Profile. However, upon surfacing, the pressure differential between the slower theoretical compartments and the ambient pressure is lower in the Shallower Decompression Profile than the one observed in the Deeper Decompression Profile, where a darker red can be spotted at the right end of the chart.

Although not necessarily comparable with this study, due to differences in methodology adopted, one previous study designed to compare results generated by different decompression profiles also reported increased levels of inflammatory markers. In this particular study, inflammation was estimated by the pre and post dive levels of chemokine (C-C motif) ligand 5 (CCl5) in profiles with deeper versus shallower decompression stops [91]. As mentioned earlier, an experiment conducted by the US Navy Experimental Diving Unit [35], although not controlling for inflammation or immune system activation markers, reported higher decompression sickness incidence when deeper decompression stops were used in the decompression profile, as well as higher average venous gas emboli counts. Even though in these two cases the protocols used were not necessarily comparable to the one used in this experiment, the published results are consistent with the findings here reported.

It is interesting to note that the Shallower Decompression Profile produced a higher post dive average SDNN increase (Figure 7). Additionally, almost a half of the volunteers that presented a reduction in the SDNN in the Deeper Decompression Profile did not present the same reduction in the Shallow Decompression Profile. Of course, these numbers must be taken with care due to the very small sample, but they might shed some light on individual response to decompression.

In the *Case Study* reported, 3 out of 4 volunteers had SDNN reduction when submitted to high supersaturation pressures throughout the whole decompression process, while presenting significant reductions in hematocrit and hemoglobin. Such erythrocytes death, as previously discussed, is possibly to be associated with higher levels of MPO expression and oxidative stress.

It seems to be too soon, however, to suggest adjustments in the decompression profile on an individual basis based on the results obtained so far. The variance in individual responses is enormous and some individuals did not show different results even when very provocative exposures were used, like the one detailed in the *Case Study*. It seems, however, that minimizing the absorption of inert gases by slower compartments, what is achieved by avoiding deeper decompression profiles, while reducing the total supersaturation upon surfacing is associated with lesser overall physiological alterations related to the compression – decompression process. In this sense, comparing individual HRV indicators after different exposure profiles might provide an opportunity for adjustments in the decompression profile according to individual responses, since, based on the results obtained by this study, HRV correlates with other physiological alterations caused by decompression-related stress.

Bibliography

1. A E Boycott, G C C Damant JSH. The Prevention of Compressed-air Illness. *J Hyg*. 1908:342-443.
2. Pollock NW. Patent Foramen Ovale : Background and Impact on Divers. 2004.
3. Liou K, Wolfers D, Turner R, et al. Patent Foramen Ovale Influences the Presentation of Decompression Illness in SCUBA Divers. *Hear Lung Circ*. 2015;24(1):26-31. doi:10.1016/j.hlc.2014.07.057
4. Fisher DC, Fisher EA, Budd JH, Rosen SE, Goldman ME. The incidence of patent foramen ovale in 1,000 consecutive patients: A contrast transesophageal echocardiography study. *Chest*. 1995;107(6):1504-1509. doi:10.1378/chest.107.6.1504
5. Eldridge MW, Dempsey JA, Haverkamp HC, Lovering AT, Hokanson JS. Exercise-induced intrapulmonary arteriovenous shunting in healthy humans. *J Appl Physiol*. 2004;97(3):797-805. doi:10.1152/japplphysiol.00137.2004
6. Doolette DJ, Upton RN, Grant C. *Altering Blood Flow Does Not Reveal Differences between Nitrogen and Helium Kinetics in Brain or in Skeletal Miracle in Sheep*. Vol 118.; 2015. doi:10.1152/japplphysiol.00944.2014
7. Stanziola A, Toulemonde M, Li Y, et al. Motion Artifacts and Correction in Multi-Pulse High Frame Rate Contrast Enhanced Ultrasound. *IEEE Trans Ultrason Ferroelectr Freq Control*. 2018;66(2):417-420.

doi:10.1109/TUFFC.2018.2887164

8. Arieli R, Marmur A. A biophysical vascular bubble model for devising decompression procedures. *Physiol Rep*. 2017;5(6):1-11. doi:10.14814/phy2.13191

9. Brubakk AO, Duplancic D, Valic Z, et al. A single air dive reduces arterial endothelial function in man. *J Physiol*. 2005;566(3):901-906. doi:10.1113/jphysiol.2005.089862

10. Thom SR, Bennett M, Banham ND, et al. Association of microparticles and neutrophil activation with decompression sickness. *J Appl Physiol*. 2015;119(5):427-434. doi:10.1152/japplphysiol.00380.2015

11. Thom SR, Milovanova TN, Bogush M, et al. Microparticle production, neutrophil activation, and intravascular bubbles following open-water SCUBA diving. *J Appl Physiol*. 2012;112(8):1268-1278. doi:10.1152/japplphysiol.01305.2011

12. Papadopoulou V, Germonpré P, Cosgrove D, et al. Variability in circulating gas emboli after a same scuba diving exposure. *Eur J Appl Physiol*. 2018;118(6):1255-1264. doi:10.1007/s00421-018-3854-7

13. Doolette DJ. Venous gas emboli detected by two-dimensional echocardiography are an imperfect surrogate endpoint for decompression sickness. *Diving Hyperb Med*. 2016;46(1):4-10.

14. Møllerløkken AOB and A. The role of intra-vascular bubbles and the vascular endothelium in decompression sickness. *Am Sci*. 2009;39(3):162-169.

15. Madden LA, Laden G. Gas bubbles may not be the underlying cause of decompression illness - The at-depth endothelial dysfunction hypothesis. *Med Hypotheses*. 2009;72(4):389-392. doi:10.1016/j.mehy.2008.11.022

16. Batool S, Abbasian N, Burton JO, Stover C. Microparticles and their roles in inflammation: A review. *Open Immunol J*. 2013;6(1):1-14. doi:10.2174/1874226201306010001

17. Ardoin SP, Shanahan JC, Pisetsky DS. The role of microparticles in inflammation and thrombosis. *Scand J Immunol*. 2007;66(2-3):159-165. doi:10.1111/j.1365-3083.2007.01984.x

18. Puddu P, Puddu GM, Cravero E, Muscari S, Muscari A. The involvement of circulating microparticles in inflammation, coagulation and cardiovascular diseases. *Can J Cardiol*. 2010;26(4):140-145. doi:10.1016/S0828-282X(10)70371-8

19. Stephen R. Thom, Veena M. Bhopale, Kevin Yu and MY. Microparticle and interleukin IL-1β production associated with human high-pressure exposures.pdf. 2018:1339-1348.

20. Thom SR, Bhopale VM, Yang M. Neutrophils generate microparticles during exposure to inert gases due to cytoskeletal oxidative stress. *J Biol Chem*. 2014;289(27):18831-18845. doi:10.1074/jbc.M113.543702

21. Olszanski R, Radziwon P, Siermontowski P, et al. Trimix instead of air, decreases the effect of short-term hyperbaric exposures on platelet and fibrinolysis activation. *Adv Med Sci*. 2010;55(2):313-316. doi:10.2478/v10039-010-0050-3

22. Yang M, Bhopale VM, Thom SR. Separating the roles of nitrogen and oxygen in high pressure-induced blood-borne microparticle elevations, neutrophil activation, and vascular injury in mice. *J Appl Physiol*. 2015;119(3):219-222. doi:10.1152/japplphysiol.00384.2015

23. Félétou M. Chapter 2 : Multiple Functions of the Endothelial Cells. *Endothel Part 1 - Mult Funct Endothel Cells—Focus Endothel Vasoact Mediat*. 2011:1-8. https://www.ncbi.nlm.nih.gov/books/NBK57148/.

24. Hadi HAR, Carr CS, Al Suwaidi J. Endothelial dysfunction: cardiovascular risk factors, therapy, and outcome. *Vasc Health Risk Manag*. 2005;1(3):183-198.

25. G Giribela CR, Gengo R, Hong V, Consolim-Colombo FM. Endothelial function and dysfunction: pathophysiology and perspectives for use in research and clinical practice. *Rev Bras Hipertens*. 2011;18(1):27-32.

26. Winterbourn CC, Kettle AJ, Hampton MB. Reactive Oxygen Species and Neutrophil Function. *Annu Rev Biochem*. 2016;85(1):765-792. doi:10.1146/annurev-biochem-060815-014442

27. Förstermann U, Sessa WC. Nitric oxide synthases: Regulation and function. *Eur Heart J*. 2012;33(7):829-837. doi:10.1093/eurheartj/ehr304

28. Theunissen S, Guerrero F, Sponsiello N, et al. Nitric oxide-related endothelial changes in breath-hold and scuba divers. *Undersea Hyperb Med*. 2013;40(2):135-144.

29. Madden LA, Chrismas BC, Mellor D, et al. Endothelial function and stress response after simulated dives to 18 msw breathing air or oxygen.

Aviat Sp Environ Med. 2010;81(1):41-45. doi:10.3357/ASEM.2610.2010

30. Theunissen S, Balestra C, Boutros A, de Bels D, Guerrero F, Germonpré P. The effect of pre-dive ingestion of dark chocolate on endothelial function after a scuba dive. *Diving Hyperb Med*. 2015;45(1):4-9.

31. Xazh V, Chrismas BCR, Midgley AW, Taylor L, Vince R V, Laden G. Acute antioxidant pre-treatment attenuates endothelial microparticle release after decompression.

32. Wisløff U, Richardson RS, Brubakk AO. NOS inhibition increases bubble formation and reduces survival in sedentary but not exercised rats. *J Physiol*. 2003;546(2):577-582. doi:10.1113/jphysiol.2002.030338

33. Madden D, Thom SR, Dujic Z. Exercise before and after SCUBA diving and the role of cellular microparticles in decompression stress. *Med Hypotheses*. 2016;86:80-84. doi:10.1016/j.mehy.2015.12.006

34. Marroni A, Bennett PB, Cronje FJ, et al. A deep stop during decompression from 82 fsw (25 m) significantly reduces bubbles and fast tissue gas tensions. *Undersea Hyperb Med*. 2004;31(2):233-243.

35. Doolette D, Gerth W, Gault K. Redistribution of decompression stop time from shallow to deep stops increases incidence of decompression sickness in air decompression dives. 2011.

36. Schirato SR, El-dash I, El-dash V, Natali JE, Starzynski PN, Chaui-berlinck JG. Heart rate variability changes as an indicator of decompression-related physiological stress. 2018:173-182.

37. Noh Y, Posada-Quintero HF, Bai Y, et al. Effect of shallow and deep

SCUBA dives on heart rate variability. *Front Physiol*. 2018;9(FEB):1-12. doi:10.3389/fphys.2018.00110

38. American TN. Task Force of the European Society of Cardiology and The North American Society of Pacing and Electrophysiology. Heart rate variability: Standards of measurement, physiological interpretation, and clinical use. *Eur Heart J*. 1996;17:354-381. doi:10.1161/01.CIR.93.5.1043

39. Acharya UR, Joseph KP, Kannathal N, Lim CM, Suri JS. Heart rate variability: A review. *Med Biol Eng Comput*. 2006;44(12):1031-1051. doi:10.1007/s11517-006-0119-0

40. Rahman F, Pechnik S, Gross D, Sewell LT, Goldstein DS. Low frequency power of heart rate variability reflects baroreflex function, not cardiac sympathetic innervation. *Clin Auton Res*. 2011;21(3):133-141. doi:10.1007/s10286-010-0098-y

41. Zhong Y, Jan KM, Ki HJ, Chon KH. Quantifying cardiac sympathetic and parasympathetic nervous activities using principal dynamic modes analysis of heart rate variability. *Am J Physiol - Hear Circ Physiol*. 2006;291(3):1475-1483. doi:10.1152/ajpheart.00005.2006

42. Malliani A, Pagani M, Lombardi F, Cerutti S. Cardiovascular neural regulation explored in the frequency domain. *Circulation*. 1991;84(2):482-492. doi:10.1161/01.CIR.84.2.482

43. Appel ML, Berger RD, Saul JP, Smith JM, Cohen RJ. Beat to beat variability in cardiovascular variables: Noise or music? *J Am Coll*

Cardiol. 1989;14(5):1139-1148. doi:10.1016/0735-1097(89)90408-7

44. Sloan RP. Heart Rate Variability Predicts Levels of Inflammatory Markers: Evidence for the Vagal Anti-Inflammatory Pathway. 2015;(Bernik 2002):94-100. doi:10.1016/j.bbi.2014.12.017.Heart

45. Adam Moser, Kevin Range and DMY. Relationship between Heart Rate Variability, Interleukin-6, and Soluble Tissue Factor in Healthy Subjects. *Bone*. 2008;23(1):1-7. doi:10.1038/jid.2014.371

46. Kaufman CL, Kaiser DR, Steinberger J, Dengel DR. Relationships between heart rate variability, vascular function, and adiposity in children. *Clin Auton Res*. 2007;17(3):165-171. doi:10.1007/s10286-007-0411-6

47. Thom SR, Yang M, Bhopale VM, Milovanova TN, Bogush M, Buerk DG. Intramicroparticle nitrogen dioxide is a bubble nucleation site leading to decompression-induced neutrophil activation and vascular injury. *J Appl Physiol*. 2013;114(5):550-558. doi:10.1152/japplphysiol.01386.2012

48. Mashayekhi G, Zahedi E, Movahedian Attar H, Sharifi F. Flow mediated dilation with photoplethysmography as a substitute for ultrasonic imaging. *Physiol Meas*. 2015;36(7):1551-1571. doi:10.1088/0967-3334/36/7/1551

49. Yu X, Xu J, Huang G, et al. Bubble-induced endothelial microparticles promote endothelial dysfunction. *PLoS One*. 2017;12(1). doi:10.1371/journal.pone.0168881

50. Bühlman A. *Decompression, Decompression Sickness*.; 1984. doi: 10.1007/978-3-662-02409-6

51. Baker EC. Understanding M-values. *Immersed*. 1998;3(3):23-27.

52. Ludbrook J, Dudley H. Why Permutation Tests Are Superior to t and F Tests in Biomedical Research Author (s): John Ludbrook and Hugh Dudley Source : The American Statistician , Vol . 52 , No . 2 (May , 1998), pp . 127-132 Published by : American Statistical Association Stab. 2008;52(2):127-132.

53. Haykin S. *Neural Networks and Machine Learning*. Vol 127. Third Edit. (Horton MJ, ed.). Pearson; 1999.

54. Smith L. A tutorial on Principal Components Analysis. *Dep Comput Sci Univ Otago*. 2006:12-28. doi:http://www.cs.otago.ac.nz/research/techreports.php

55. Likas A, Vlassis N, J. Verbeek J. The global k-means clustering algorithm. *Pattern Recognit*. 2003;36(2):451-461. doi:10.1016/S0031-3203(02)00060-2

56. Lau D, Mollnau H, Eiserich JP, et al. Myeloperoxidase mediates neutrophil activation by association with CD11b/CD18 integrins. *Proc Natl Acad Sci U S A*. 2005;102(2):431-436. doi:10.1073/pnas.0405193102

57. Marchitto N, Iannarelli N, Paparello PT, et al. The Cardiovascular risk in the scubadiver. *J Sports Med Phys Fitness*. 2019;59(10):1779-1782. doi:10.23736/S0022-4707.19.09358-7

58. Lauscher P, Kertscho H, Enselmann P, Lauscher S, Habler O, Meier J. Effects of alterations of inspiratory oxygen fractions on heart rate variability. *Br J Anaesth*. 2012;108(3):402-408. doi:10.1093/bja/aer404

59. Thom SR, Ma M, Bhopale VM, Zhou C, Mao L. Oxidative stress mediated by nitrogen at elevated pressure inhibits non-small cell lung cancer growth. *Exp Lung Res*. 2017;43(4-5):175-180. doi:10.1080/01902148.2017.1331478

60. Strauss MB, Lu LQ, Miller SS. The Gradient Perfusion Model Part 1: Why and at what sites decompression sickness can occur. *Undersea Hyperb Med*. 2018;45(3):287-295.

61. Strauss MB, Lu LQ, Miller SS. The Gradient Perfusion Model Part 2: Substantiation of the GPM with clinical cases. *Undersea Hyperb Med*. 2018;45(3):297-305.

62. Lu LQ, Strauss MB, Miller SS. The Gradient Perfusion Model Part 3: An extraordinary case of decompression sickness. *Undersea Hyperb Med*. 2018;45(3):307-311.

63. Thom SR, Milovanova TN, Bogush M, et al. Bubbles, microparticles, and neutrophil activation: Changes with exercise level and breathing gas during open-water SCUBA diving. *J Appl Physiol*. 2013;114(10):1396-1405. doi:10.1152/japplphysiol.00106.2013

64. Bai Y, Mahon RT, White JC, Brink PR, Chon KH. Impairment of the autonomic nervous function during decompression sickness in swine. *J Appl Physiol*. 2009;106(3):1004-1009.

doi:10.1152/japplphysiol.91246.2008

65. Bai Y, Selvaraj N, Petersen K, et al. The autonomic effects of cardiopulmonary decompression sickness in swine using principal dynamic mode analysis. *Am J Physiol - Regul Integr Comp Physiol*. 2013;305(7):748-758. doi:10.1152/ajpregu.00150.2012

66. Agelink MW, Majewski TB, Andrich J, Mueck-Weymann M. Short-term effects of intravenous benzodiazepines on autonomic neurocardiac regulation in humans: A comparison between midazolam, diazepam, and lorazepam. *Crit Care Med*. 2002;30(5):997-1006. doi:10.1097/00003246-200205000-00008

67. Alexander Haensel, Paul J. Mills, Richard A. Nelesen, Michael G. Ziegler, Joel E. Dimsdale. The relationship between heart rate variability and inflammatory markers in cardiovascular diseases. *Psychoneuroendocrinology*. 2012;76(October 2009):211-220. doi:10.1007/s11103-011-9767-z.Plastid

68. Pinter A, Horvath T, Sarkozi A, Kollai M. Relationship between heart rate variability and endothelial function in healthy subjects. *Auton Neurosci Basic Clin*. 2012;169(2):107-112. doi:10.1016/j.autneu.2012.05.005

69. Teixeira BC, Lopes AL, Macedo RCO, et al. Inflammatory markers, endothelial function and cardiovascular risk. *J Vasc Bras*. 2014;13(2):108-115. doi:10.1590/jvb.2014.054

70. Aratani Y. Myeloperoxidase: Its role for host defense, inflammation, and

neutrophil function. *Arch Biochem Biophys*. 2018;640(December 2017):47-52. doi:10.1016/j.abb.2018.01.004

71. Lau D, Baldus S. Myeloperoxidase and its contributory role in inflammatory vascular disease. *Pharmacol Ther*. 2006;111(1):16-26. doi:10.1016/j.pharmthera.2005.06.023

72. Dalton JA, Higgins MK, Miller AH, Keefe FJ, Khuri FR. Myeloperoxidase: A new player in autoimmunity.HHS Public Access. *Cell Immunol*. 2016;38(5):457-464. doi:10.1097/COC.0b013e3182a79009.Pain

73. Summers C, Rankin SM, Condliffe AM, Singh N, Peters AM, Chilvers ER. Neutrophil kinetics in health and disease. *Trends Immunol*. 2010;31(8):318-324. doi:10.1016/j.it.2010.05.006

74. Verma S, Wang CH, Li SH, et al. A self-fulfilling prophecy: C-reactive protein attenuates nitric oxide production and inhibits angiogenesis. *Circulation*. 2002;106(8):913-919. doi:10.1161/01.CIR.0000029802.88087.5E

75. Alicia P, Yourish K. Platelets: versatile effector cells in hemostasis, inflammation, and the immune continuum. *Nyt*. 2018;34(1):5-30. doi:10.1007/s00281-011-0286-4

76. Lindemann S, Tolley ND, Dixon DA, et al. Activated platelets mediate inflammatory signaling by regulated interleukin 1β synthesis. *J Cell Biol*. 2001;154(3):485-490. doi:10.1083/jcb.200105058

77. Pontier JM, Vallée N, Bourdon L. Bubble-induced platelet aggregation in

a rat model of decompression sickness. *J Appl Physiol*. 2009;107(6):1825-1829. doi:10.1152/japplphysiol.91644.2008

78. Pontier JM, Blatteau JE, Vallée N. Blood platelet count and severity of decompression sickness in rats after a provocative dive. *Aviat Sp Environ Med*. 2008;79(8):761-764. doi:10.3357/ASEM.2299.2008

79. Pontier JM, Jimenez C, Blatteau JE. Blood platelet count and bubble formation after a dive to 30 msw for 30 min. *Aviat Sp Environ Med*. 2008;79(12):1096-1099. doi:10.3357/ASEM.2352.2008

80. Michael Jacey, Alfonso Gonzales DT. *Hematologic Changes after Two Exposures to 6.7ATA Air at Three-Day Intervals*.; 1977.

81. Stokes KY, Granger DN. Platelets: A critical link between inflammation and microvascular dysfunction. *J Physiol*. 2012;590(5):1023-1034. doi:10.1113/jphysiol.2011.225417

82. Gorudko I V., Sokolov A V., Shamova E V., et al. Myeloperoxidase modulates human platelet aggregation via actin cytoskeleton reorganization and store-operated calcium entry. *Biol Open*. 2013;2(9):916-923. doi:10.1242/bio.20135314

83. Hottz ED, Lopes JF, Freitas C, et al. Platelets mediate increased endothelium permeability in dengue through NLRP3-inflammasome activation. *Blood*. 2013;122(20):3405-3414. doi:10.1182/blood-2013-05-504449

84. Cognasse F, Hamzeh-Cognasse H, Laradi S, et al. The role of microparticles in inflammation and transfusion: A concise review.

Transfus Apher Sci. 2015;53(2):159-167. doi:10.1016/j.transci.2015.10.013

85. Vince R V., McNaughton LR, Taylor L, Midgley AW, Laden G, Madden LA. Release of VCAM-1 associated endothelial microparticles following simulated SCUBA dives. *Eur J Appl Physiol*. 2009;105(4):507-513. doi:10.1007/s00421-008-0927-z

86. Perovic A, Nikolac N, Njire Braticevic M, et al. Does recreational scuba diving have clinically significant effect on routine haematological parameters? *Biochem Med*. 2017;27(39):27-38. https://www.ncbi.nlm.nih.gov/pmc/articles/PMC5493166/pdf/bm-27-325.pdf.

87. Gunes AE, Aktas S. Effect of hyperbaric oxygen therapy on complete blood count. *Undersea Hyperb Med*. 2017;44(4):357-364. doi:10.22462/7.8.2017.8

88. Elayan IM, Axley MJ, Prasad P V., Ahlers ST, Auker CR. Effect of hyperbaric oxygen treatment on nitric oxide and oxygen free radicals in rat brain. *J Neurophysiol*. 2000;83(4):2022-2029.

89. Chapleau MW, Li Z, Meyrelles SS, Ma X, Abboud FM. Mechanisms Determining Sensitivity of Baroreceptor Afferents in Health and Disease. *Ann N Y Acad Sci*. 2006;940(1):1-19. doi:10.1111/j.1749-6632.2001.tb03662.x

90. Harris KF, Matthews KA. Interactions between Autonomic Nervous System Activity and Endothelial Function: A Model for the Development

of Cardiovascular Disease. *Psychosom Med*. 2004;66(2):153-164. doi:10.1097/01.psy.0000116719.95524.e2

91. Spisni E, Marabotti C, De Fazio L, et al. A comparative evaluation of two decompression procedures for technical diving using inflammatory responses: Compartmental versus ratio deco. *Diving Hyperb Med*. 2017;47(1):9-16. doi:10.28920/dhm47.1.9-16

Appendix I

Flow cytometry gates definition Immunophenotyping

CD45+ Debris Exclusion Single Cells – FSC Single Cell SSC

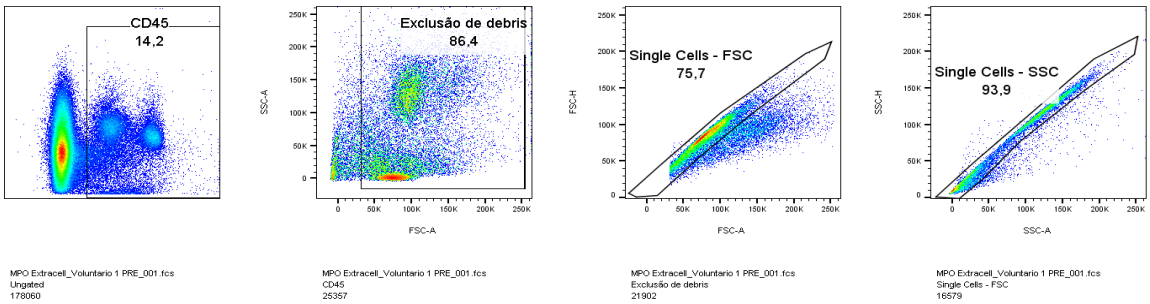

Live Cells CD3- CD19 SSC High CD14- CD16 MPO+

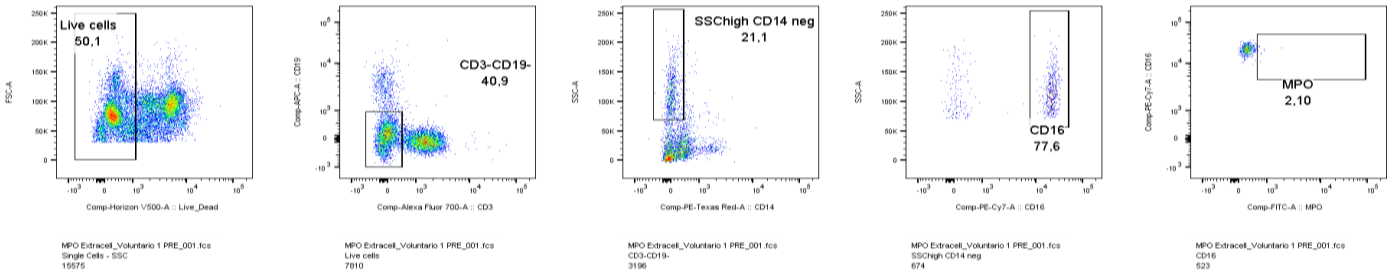

Flow cytometry gates definition for Microparticles analysis

Annexin + MPs CD66b+ MPs CD31+/CD41+

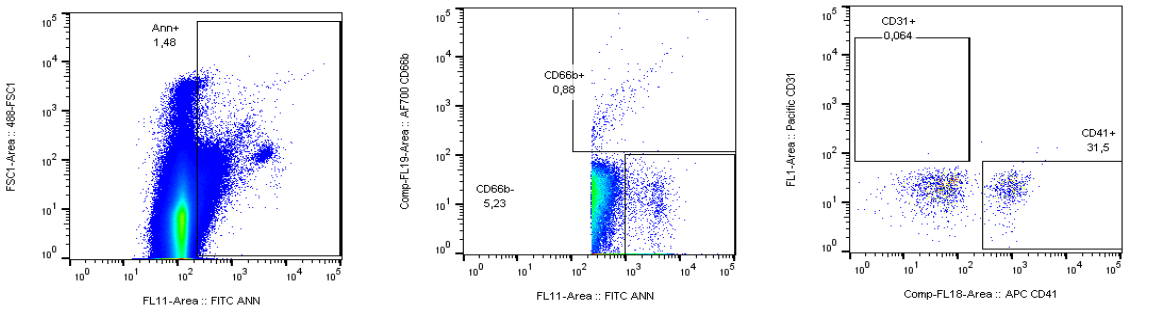

Appendix II

Principal Component Analysis - Deeper Decompression Profile

	PC1	PC2	PC3	PC4	PC5	PC6	PC7	PC8
CD16	-0,47	0,08	-0,07	0,51	-0,14	-0,08	-0,69	0,03
MPO (%)	-0,52	0,14	-0,20	0,11	-0,20	-0,13	0,54	0,55
MPO(MFI)	-0,31	0,17	-0,49	-0,24	0,47	0,59	-0,07	-0,09
Annexin+	-0,48	0,29	0,37	-0,05	-0,05	-0,09	0,28	-0,68
MP CD66b+	0,29	0,33	0,22	0,68	0,09	0,48	0,25	0,04
MP CD31+	0,21	0,42	-0,33	-0,19	-0,75	0,20	-0,08	-0,14
MP CD41+	0,03	0,64	0,43	-0,35	0,20	-0,09	-0,26	0,40
SDNN Ratio	0,24	0,41	-0,49	0,21	0,33	-0,59	0,08	-0,19

Principal Component Analysis - Shallower Decompression Profile

	PC1	PC2	PC3	PC4	PC5	PC6	PC7	PC8
CD16	0,62	-0,08	0,29	-0,03	0,18	-0,24	-0,05	0,66
MPO (%)	0,64	-0,21	0,15	-0,03	0,05	0,14	0,32	-0,63
MPO(MFI)	-0,19	-0,59	-0,30	-0,17	0,18	0,20	0,58	0,30
Annexin+	-0,19	-0,42	0,42	0,20	0,46	0,39	-0,45	-0,07
MP CD66b+	-0,06	-0,13	0,41	-0,65	-0,55	0,27	-0,09	0,08
MP CD31+	0,28	0,36	-0,42	-0,17	0,16	0,71	-0,18	0,15
MP CD41+	-0,15	0,42	0,50	0,34	-0,01	0,33	0,54	0,16
SDNN Ratio	-0,17	0,32	0,16	-0,61	0,63	-0,22	0,12	-0,14

Appendix III

Figure 1, below, plotted the average bubble count generated by two different decompression profiles, according to DAN Europe observations. For the purpose of this comparison, the volunteer's observations were paired based on the data available.

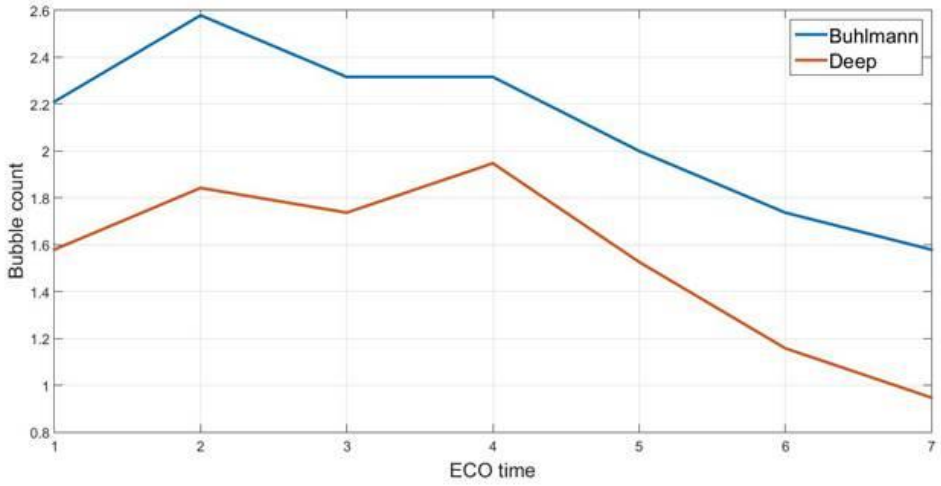

Figure 1. Bubble grades observed after dive for two different profiles

The plot below (figure 2) is the estimated bubble grade count produced by the model developed in the Laboratory of Energetics and Theoretical Physiology of the University of Sao Paulo, using the parameters of the profile named "Bühlman" in the dataset (which cannot be compared to neither one of the profiles used in the present study). Time (in the x-axis) is given in minutes, being zero the start of the bottom phase of the dive, therefore the end of the dive happens slightly before the 80´mark. As it can be noticed, according to the model, bubbles will peak approximately 15´ after the end of the dive and will reach a maximum value of approximately 600 in our arbitrary scale (y-axis).

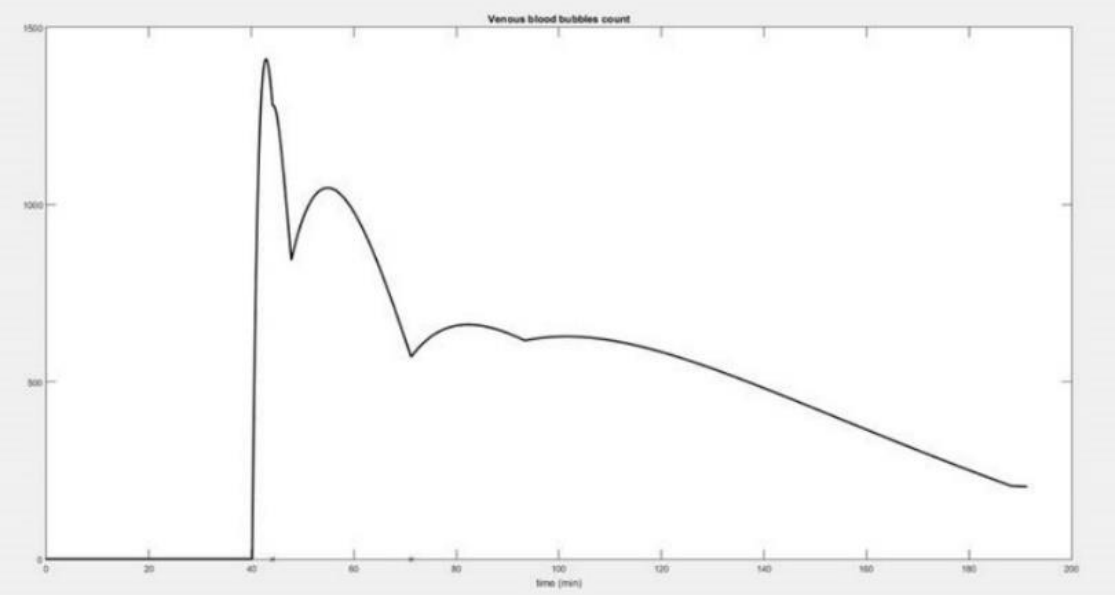

Figure 2. Bubble grades estimated by the model after the “Bühlman” profile

Figure 3, below, was produced by the model using the parameters of the profile named “Deep” (which is approximately the same of the Deep Decompression Profile described in the present study). Again, time is given in minutes after the start of the bottom phase of the dive, being the end of the dive around minute 80. What is interesting here is that, according to the model, bubble count would peak around 50 minutes after the end of the dive, producing a maximum bubble grade of 440 in our arbitrary scale. Please notice that it is 1.35 times less than what was predicted for the Bühlman profile, which is exactly the same difference between the maximum average grades actually observed in the original dataset. Additionally, the post dive interval before reaching the peak predicted by the model is compatible with actual observations.

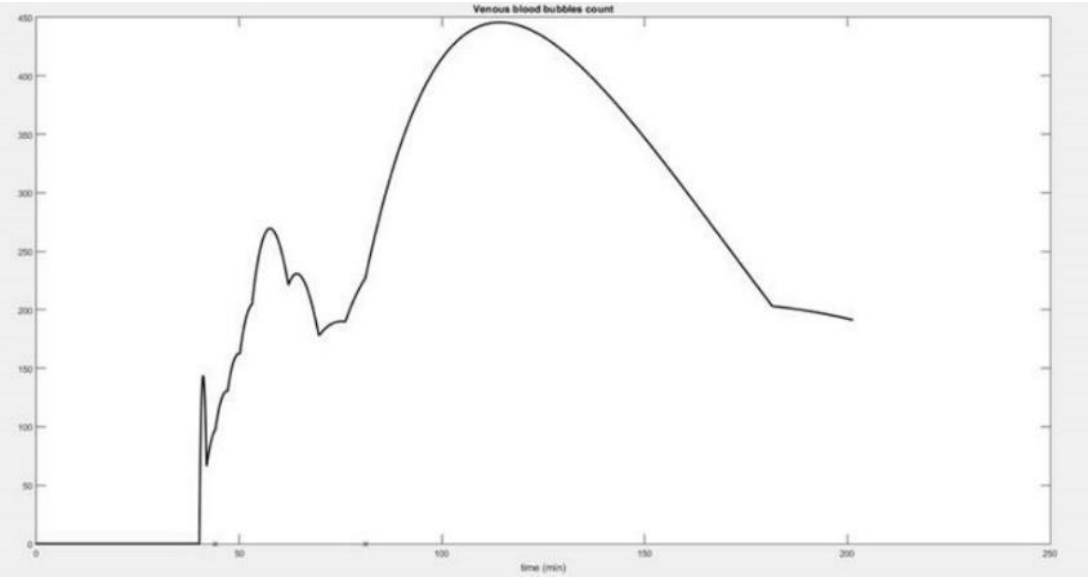

Figure 3. Bubble grades estimated by the model after the “Deep” profile

Appendix IV

Normalized Variation Rates

Volunteer	CD16 (%)	MPO (%)	MPO (MFI)	Anexx +	MP CD66b +	MP CD31 +	MP CD41 +
1	0,32940118	0,35870686	0,5996493	0,096725061	0,08673344	0,8312281	0,084553867
2	0,30228838	0,3815415	0,8187024	0,223481996	0,16156652	0,8017544	0,731344682
3	0,36851677	0,44628598	0,4273111	0,546082061	0,27464463	0,7063158	0,325669516
4	0,30525701	0,32813343	0,2029454	0,187289218	0,05746691	0,7385965	0,008732186
5	0,32303583	0,39873498	0,4191251	0,178284257	0,29976389	0,7315789	0,969861213
6	0,35601047	0,42522653	0,3277384	0,411754561	0,26346045	0,7315789	0,152426866
7	0,26323436	0,16372946	0,5697159	0,015926894	0,01692215	0,6561404	0,240323368
8	0,38487598	0,06083405	0,6593388	0,177754219	0,17285236	0,7333333	0,073829781
9	0,26778926	0,02190821	0,4180908	0,386643169	0,50409138	0,7224561	0,547636694
10	0,29026371	0,21058423	0,3420329	0,294735894	0,04220813	0,7315789	0,310904477
11	0,23095516	0,18535807	0,3893209	0,137681044	0,22501893	0,7387719	0,108470314
12	0,25236137	0,26256854	0,3594309	0,202984743	0,08918682	0,7292982	0,132256913
13	0,25069713	0,29510815	0,5339333	0,565631597	0,11903861	0,7266667	0,487031265
14	0,15050283	0,18378959	0,5022839	0,111605546	0,09408799	0,7245614	0,266648545
15	0,38050737	0,5339785	0,5070314	1	0,13400723	0,7333333	1
16	0,16675499	0,2037003	0,6509561	0,433099467	0,02471578	0,7631579	0,900153759
17	0,41326218	0,32536764	0,626453	0,425461115	0,1172232	0,7327456	0,36556685
18	0,24996291	0,34412666	0,6180691	0,017243274	0,41321448	0,7263158	0,071708653
19	0,35272747	0,73986344	0,7243401	0,684644229	0,03926388	0,7315789	0,152673516
20	0,36364966	0,56198419	0,5981417	0,475518245	0,08236004	0,7392982	0,057534317
21	0,40678102	0,789013	1	0,640891927	0,01995647	0,7191228	0,00334241
22	0,24525483	0,14293206	0,4639926	0,16642242	0,08402725	0,7824561	0,196797319
23	0,24392542	0,18075295	0,378446	0,420880623	0,17947487	0,7491228	0,283609552
24	0,25809517	0,22307746	0,4991855	0,286749193	0,29710711	0,9631579	0,60192986
25	0,21096035	0,2505156	0,4077591	0,026200732	0,24449596	0,8912281	0,258560318
26	0,2133531	0,07071317	0,69387	0,217901271	0,27932869	0,7087719	0,27034713
27	0	0,1468508	0,7860824	0,026479942	0,21451589	0,7315789	0
28	0,08803555	0,15697673	0,6958651	0,353012254	0	0,7596491	0,103149463
29	1	1	0,4045656	0,287056324	0,23387585	0,7387719	0,032560007
30	0,24796824	0,21046464	0	0	0,5032147	0,7305263	0,426610116
31	0,19267995	0,08016076	0,4669651	0,638050129	0,08856576	0,7315789	0,149569481
32	0,29528108	0,06032138	0,5628184	0,213835314	0,07381561	0,7315789	0,122326287
33	0,28785352	0,08210046	0,470086	0,358879769	0,47642227	0,7315789	0,182180514
34	0,24100152	0	0,2393017	0,20426974	0,17081785	0,715614	0,148764779
35	0,20674041	0,27900436	0,6100565	0,300538718	0,07406847	0,7296491	0,171783058
36	0,30986882	0,26733211	0,2723663	0,576479206	0,0723568	0,7284895	0,213461492
37	0,28806374	0,32955903	0,5865873	0,699852671	0,00995561	0,7377193	0,30953329
38	0,26230618	0,33990741	0,672049	0,538438348	1	0,7315789	0,154237781
39	0,2398156	0,21566745	0,5737592	0,830593803	0,705062	0,6385965	0,158058798
40	0,22906209	0,11179397	0,4746428	0,388863545	0,10253325	0,7315789	0,191973067
41	0,19970868	0,05675923	0,6449371	0,732125206	0,49735575	0	0,169128549
42	0,26390791	0,22629196	0,4614064	0,005813568	0,39912945	0,7577193	0,054963822
43	0,25392208	0,20219536	0,3360224	0,112086706	0,27552875	1	0,298783615
44	0,29041685	0,12394608	0,294023	0,139113154	0,28242493	0,5929825	0,243307991
45	0,22281965	0,17284942	0,3335153	0,345429309	0,19967082	0,7964912	0,098553741
46	0,24901583	0,23792916	0,4307449	0,09760829	0,42872238	0,7789474	0,084789506
47	0,24862637	0,17013874	0,3393167	0,422510705	0,26219615	0,554386	0,432043756

Appendix IV

Observed Variation Rates

Volunteer	CD16 (%)	MPO (%)	MPO (MFI)	Anexx +	MP CD66b +	MP CD31 +	MP CD41 +
1	1,236180905	1,123287671	1,025528169	0,638157895	0,710144928	0,568	0,568690096
2	1,153061224	1,1875	1,212343096	0,921568627	1,203389831	0,4	4,817708333
3	1,356097561	1,369565217	0,878552972	1,642857143	1,948717949	-0,144	2,152671756
4	1,162162162	1,037313433	0,687207296	0,840646651	0,517241379	0,04	0,070588235
5	1,216666667	1,235849057	0,87157173	0,820512821	2,114285714	0	6,384615385
6	1,317757009	1,310344828	0,793634497	1,342519685	1,875	0	1,014573991
7	1,033333333	0,575	1	0,457504521	0,25	-0,43	1,592
8	1,40625	0,285652174	1,076433121	0,819327731	1,277777778	0,01	0,498239437
9	1,047297297	0,176190476	0,870689655	1,286374134	3,461063041	-0,052	3,610859729
10	1,116197183	0,706758305	0,805825243	1,080882353	0,416666667	0	2,055674518
11	0,934375	0,635820896	0,846153846	0,72972973	1,621621622	0,041	0,725806452
12	1	0,852941176	0,820662768	0,875739645	0,726315789	-0,013	0,882069795
13	0,994897959	0,944444444	0,969483568	1,686567164	0,923076923	-0,028	3,212719298
14	0,687732342	0,631410256	0,942492013	0,671428571	0,75862069	-0,04	1,764940239
15	1,392857143	1,616161616	0,946540881	2,657754011	1,02173913	0,01	6,582608696
16	0,737556561	0,687400319	1,069284065	1,390243902	0,301369863	0,18	5,926680244
17	1,493273543	1,029535865	1,048387097	1,373165618	0,911111111	0,00665	2,414772727
18	0,992647059	1,082287308	1,041237113	0,460447761	2,862068966	-0,03	0,484304933
19	1,307692308	2,195121951	1,131868132	1,952662722	0,397260274	0	1,016194332
20	1,341176471	1,694915254	1,024242424	1,485086342	0,681318681	0,044	0,391188251
21	1,473404255	2,333333333	1,366959064	1,85483871	0,27	-0,071	0,035180723
22	0,978213508	0,516516517	0,909836066	0,793991416	0,692307692	0,29	1,306060606
23	0,974137931	0,622871046	0,836879433	1,362924282	1,321428571	0,1	1,876363636
24	1,017578125	0,741889986	0,939849624	1,06302521	2,096774194	1,32	3,967532468
25	0,873076923	0,819047619	0,861878453	0,480475382	1,75	0,91	1,711805556
26	0,880412371	0,313432836	1,105882353	0,909090909	1,979591837	-0,13	1,789237668
27	0,226335878	0,527536232	1,18452381	0,481099656	1,552393273	0	0,01322314
28	0,496226415	0,556010929	1,107583774	1,211180124	0,138461538	0,16	0,690851735
29	3,292035398	2,926640927	0,85915493	1,063711911	1,68	0,041	0,227122381
30	0,986531987	0,706422018	0,514129444	0,421894219	3,455284553	-0,006	2,815789474
31	0,8170347	0,34	0,912371134	1,848484848	0,722222222	0	0,995802728
32	1,131578947	0,284210526	0,994117647	0,9	0,625	0	0,816831683
33	1,10880829	0,345454545	0,91503268	1,224299065	3,278688525	0	1,210037175
34	0,965174129	0,114583333	0,718213058	0,878612717	1,264367816	-0,091	0,990516333
35	0,86013986	0,899159664	1,03440367	1,093856655	0,626666667	-0,011	1,141732283
36	1,176300578	0,866336634	0,746411483	1,710820896	0,615384615	-0,01761	1,415533981
37	1,109452736	1,041322314	1,014388489	1,986666667	0,204081633	0,035	2,046666667
38	1,030487805	1,070422535	1,087272727	1,625766871	6,72972973	0	1,026470588
39	0,961538462	0,721052632	1,003448276	2,278985507	4,785714286	-0,53	1,051572327
40	0,928571429	0,428954424	0,918918919	1,291338583	0,814285714	0	1,274368231
41	0,838582677	0,274193548	1,064150943	2,058823529	3,416666667	-4,17	1,124293785
42	1,03539823	0,750929368	0,907630522	0,434892541	2,769230769	0,149	0,374301676
43	1,004784689	0,683168317	0,800699301	0,672504378	1,954545455	1,53	1,976047904
44	1,116666667	0,463126844	0,764880952	0,732931727	2	-0,79	1,611607143
45	0,909433962	0,600645856	0,798561151	1,194225722	1,454545455	0,37	0,660660661
46	0,98974359	0,783653846	0,881481481	0,64013267	2,964285714	0,27	0,570238095
47	0,988549618	0,593023256	0,803508772	1,366568915	1,866666667	-1,01	2,851485149